Mixing-layer-height-referenced ozone vertical distribution in the lower troposphere of Chinese megacities: Stratification, classification, meteorological, and photochemical mechanisms

Zhiheng Liao[a, b], Meng Gao[c], Jinqiang Zhang[d, e], Jiaren Sun[f], Jiannong Quan[a], Xingcan Jia[a], Yubing Pan[a], Shaojia Fan[b, g]

[a] Institute of Urban Meteorology, Chinese Meteorological Administration, Beijing, China

[b] School of Atmospheric Sciences, Sun Yat-Sen University, Zhuhai, China

[c] Department of Geography, Hong Kong Baptist University, Hong Kong SAR, China

[d] Key Laboratory of Middle Atmosphere and Global Environment Observation, Institute of Atmospheric Physics, Chinese Academy of Sciences, Beijing, China

[e] College of Earth and Planetary Sciences, University of Chinese Academy of Sciences, Beijing 100049, China

[f] Key Laboratory of Urban Ecological Environmental Simulation and Protection of Ministry of Environmental Protection, South China Institute of Environmental Sciences, Ministry of Ecology and Environment of the PRC, Guangzhou, China

[g] Guangdong Provincial Observation and Research Station for Climate Environment and Air Quality Change in the Pearl River Estuary, Key Laboratory of Tropical Atmosphere–Ocean System, Ministry of Education, Southern Marine Science and Engineering Guangdong Laboratory (Zhuhai), Zhuhai, China

Corresponding author: S. J. Fan (eesfsj@mail.sysu.edu.cn)

Abstract: Traditional tropospheric ozone (O_3) climatology uses a simple average substantially smoothed stratification structure in individual O_3 profiles, limiting our ability to properly describe and understand how O_3 is vertically distributed at the interface between the mixing layer (ML) and free troposphere (FT). In this study, we collected 1,897 ozonesonde profiles from two Chinese megacities (Beijing and Hong Kong) over the period 2000–2022 to investigate climatological vertical heterogeneity of lower-tropospheric O_3 distribution with a mixing-layer-height-referenced (*h*-referenced) vertical coordinate system. The mixing layer height (*h*) was first estimated following an integral method that integrates the information of temperature, humidity, and cloud. After that, a so-called *h*-referenced vertical distribution of O_3 was determined by averaging all individual profiles expressed as a function of z/h rather than z (where z is altitude). We found that the vertical stratification of O_3 is distributed heterogeneously in the lower troposphere, with stronger vertical gradients at the surface layer and ML–FT interface. There are low vertical autocorrelations of O_3 between the ML and FT, but high autocorrelations within each of the two atmospheric compartments. These results suggest that the ML–FT interface acts as a geophysical "barrier" separating air masses of distinct O_3 loadings. This barrier effect varies with season and city, with an ML-to-FT detrainment barrier in summer (autumn) and an FT-to-ML entrainment barrier in other seasons in Beijing (Hong Kong). Based on Student's *t* test, daily *h*-referenced O_3 profiles were further classified into three typical patterns: MLO_3-dominated, FTO_3-dominated, and uniform distribution. Although the FTO_3-dominated pattern occurs most frequently during the whole study period (69% and 54% of days in Beijing and Hong Kong, respectively), the MLO_3-dominated pattern prevails in the photochemical active season, accounting for 47% of summer days in Beijing and 54% of autumn days in Hong Kong. These occurrences of the MLO_3-dominated pattern are significantly more frequent than in previously reported results at northern mid-latitudes, indicating intensive photochemical MLO_3 production under the high-emission background of Chinese megacity. From FTO_3-dominated to MLO_3-dominated pattern, the O_3 precursor CH_2O (NO_2) experiences a substantial increase (decrease) in Beijing,

but a slight ~~increase (decrease)~~change in Hong Kong. Vertically, the increment of CH_2O is larger in the upper ML and the decrement of NO_2 is larger in the lower ML. Such vertical changes in O_3 precursors push O_3 production sensitivity away from the VOC-limited regime and facilitate high-efficiency production of O_3 via photochemical reactions, particularly in the upper ML of Beijing.

1 Introduction

Ozone (O_3), the dominant precursor of hydroxyl radicals, plays a crucial role in tropospheric chemistry. It is also an important greenhouse gas closely related to climate change and environmental issues (Seinfeld and Pandis, 2016;Monks et al., 2015). Being an air pollutant, O_3 can influence air quality on a hemispheric scale, exerting detrimental effects on human health and vegetation (Fleming et al., 2018;Mills et al., 2018). Tropospheric O_3 is primarily formed through a complex series of photochemical reactions between nitrogen oxides (NOx) and volatile organic compounds (VOCs) in the presence of sunlight (Seinfeld and Pandis, 2016). There are substantial emissions of NOx and VOCs in urban regions, where most of the population and industry are concentrated. As a result, elevated O_3 concentrations in the lower troposphere remain a persistent environmental problem in urban regions around the world (Lu et al., 2018). Significant efforts have been made to understand O_3 pollution in different cities (Monks et al., 2015). However, most previous studies were based on ground-based observations, and gave only limited insight into O_3 vertical distribution.

O_3 vertical distribution in the lower troposphere can provide very important information for mechanistic understanding of surface O_3 pollution (He et al., 2021;Lin et al., 2010;Jaffe, 2011;Yates et al., 2017). One of the major advantages when dealing with O_3 profile data is able to discriminate the two specific O_3 components corresponding to the two "reservoirs"—the mixing layer (ML) and the free troposphere (FT)—and therefore, to determine the direction and intension of vertical exchange processes across the ML-FT interface. Several studies have been made trying to resolve the O_3 vertical exchange problem in the lower troposphere (Neuman et al., 2012;Berkes et al., 2016;Kaser et al., 2017;Trousdell et al., 2016;Zhao et al., 2019;Lin et al., 2010;Zhu et al., 2020). For example, based on tethered ozone soundings during a four-day ozone episode in southern Taiwan, Lin et al. (2010) revealed that the increase rate of surface O_3 concentration due to the downward mixing of the O_3 from the O_3 reservoir layers can be as high as 12–24 ppbv h^{-1} in the late morning. Based on 214 aircraft vertical profiles in Colorado during summer 2014, Kaser et al. (2017) investigated the O_3 vertical gradient between the ML and the FT in order to estimate the FT-to-ML O_3 entrainment and to evaluate its representation in the WRF-Chem model. Their study focusing on the O_3 entrainment highlighted deficiencies in the model, indicating an overestimation of the O_3 entrainment and a too-efficient vertical mixing in the lower ML. These deficiencies were found to originate mainly from errors in the entrainment rate and ML height during the morning and an erroneous representation of the O_3 gradient at the ML–FT interface during the rest of the day. Overall, by measuring the specific terms in the vertical O_3 budget, detailed comparisons with photochemical models can uncover distinct weaknesses in current models and discern whether the difficulties lie in dynamical (transport) or chemical aspects of the numerical efforts (Trousdell et al., 2016).

O_3 vertical stratification below and above the ML-FT interface (i.e., the mixing layer height, h) is the basis for ozone vertical exchange processes. The formation of O_3 stratification is mainly due to the fact that the turbulent-convective ML and overlaying FT are usually separated by the mixing layer capping inversion, which acts as a transport barrier (Donnell et al., 2001). This barrier is indicated by steep vertical gradients of meteorological variables and chemical constituents (Petetin et al., 2018;Wyngaard and Brost, 1984;Williams et al., 2011). This means that climatological h-referenced O_3 vertical distribution in the lower troposphere could provide a useful

reference for understanding vertical exchange processes and validating air quality numerical models. However, tropospheric O_3 climatology is traditionally formed in a sea-level-referenced vertical coordinate system (Ding et al., 2008;Liao et al., 2021;Diab et al., 2004;Yonemura et al., 2002;Stauffer et al., 2016). Owing to day-to-day variation in the mixing layer top height, vertical stratification introduced in all individual profiles can be substantially smoothed in climatological profile when adopting the traditional vertical coordinate system. To address this issue, Petetin et al. (2018) proposed *h*-referenced climatology of lower-tropospheric O_3 profiles based on aircraft and ozonesondes at northern mid-latitudes over 1994–2016. When adopting this *h*-referenced vertical coordinate system, O_3 vertical stratification can be well preserved in lower-tropospheric O_3 climatology, demonstrating a significant improvement in capturing possible specific features (i.e., stratification) in the O_3 vertical distribution that would be smoothed with a simple average, in particular at the ML–FT interface. However, the *h*-referenced O_3 climatology in Petetin et al. (2018) is a hemispheric-scale composite result, which cannot represent the state over polluted urban regions, including megacities.

O_3 pollution has long been a significant environmental issue in China, despite the 2013 Clean Air Action Plan. In recent photochemical active seasons, O_3 overtook fine particles as the most important air pollutant in the three major city agglomerations: the North China Plain (NCP), the Yangtze River Delta (YRD), and the Pearl River Delta (PRD). As such, urban O_3 pollution is becoming a priority for scientific research and control strategies in China (Lu et al., 2018;Wang et al., 2022b), and numerous studies have explored the spatiotemporal characteristics and formation mechanisms of surface O_3 pollution, as summarized in Wang et al. (2017) and Wang et al. (2022b). Moreover, there are ongoing efforts to understand the role of vertical exchange in surface O_3 pollution in China based on vertical observations from tower-based, tethered-balloon-based, unmanned-aerial-vehicle-based, aircraft-based, and lidar-based observations (Lin et al., 2010;Zhao et al., 2019;He et al., 2021;Benish et al., 2020;Zhu et al., 2020;Han et al., 2020;Chen et al., 2023). These vertically observational studies generally indicate that merging of the stable boundary layer, residual layer, and convection-driven mixing layer involves the mixing of trace gases from these different atmospheric layers, and leads to complex vertical O_3 profiles. However, these existing O_3 vertical observations suffer from low observation height (tower-based, tethered-balloon-based, unmanned-aerial-vehicle-based observations), short observation period (tethered-balloon-based, aircraft-based, unmanned-aerial-vehicle-based observations), and low observation accuracy (lidar-based observation), making them less able to provide a complete and accurate O_3 vertical distribution for the whole lower troposphere, not to mention *h*-reference lower-tropospheric O_3 climatology.

To our knowledge, ozonesonde represents the most accurate observation method for O_3 profiles in the troposphere. Therefore, in this study, we collected ozonesonde data observed in Beijing (northern China, Fig. 1a) and Hong Kong (southern China, Fig. 1a) to investigate the *h*-reference O_3 vertical distribution in the lower troposphere over Chinese megacities. In addition, we also considered satellite-based O_3 precursor data, atmospheric composition reanalysis data, an integral method to determine the mixing layer top height *h*, and a photochemical indicator method to diagnose the O_3 production sensitivity. The specific aims of the study were to explore (1) the degree to which lower-tropospheric O_3 over megacities stratifies in the *h*-reference vertical coordinate system; (2) patterns in lower-tropospheric O_3 profiles in the *h*-reference vertical coordinate system; (3) how meteorological and photochemical processes modulate O_3 vertical distribution patterns in the lower troposphere; and (4) differences in the characteristics and mechanisms of lower-tropospheric O_3 vertical distribution between Beijing and Hong Kong. These results of this study offer a reference for better understanding O_3 pollution in urban regions.

2 Data and methods

2.1 Ozonesonde measurements

We used ozonesonde data collected by the Beijing Nanjiao Observatory (116.47°E, 39.80°N, 33 m) and Hong Kong King's Park Observatory (114.17°E, 22.31°N, 66 m) from 2000 to 2022 (Fig. 1). Beijing Nanjiao Observatory is located in southern suburban of Beijing (Fig. 1b), while Hong Kong King's Park Observatory is situated within the urban core of Hong Kong (Fig. 1c). Both sites are affected by urban traffic emissions (Fig. 1b and c). Ozonesondes accompanied by radiosondes were regularly launched at approximately 13:30 local standard time (LST) once a week and provided high vertical resolution profiles of O_3, temperature, pressure, and humidity. We excluded data from ozonesondes launched outside a time window of 12:00–15:00 LST in order to minimizes changes in mixing layer O_3 arising from different launch times. We interpolated the original profiles on a fixed vertical grid of 20 m vertical resolution. To reduce uncertainties associated with data gaps, we further discarded (i) profiles with > 25% missing data between 0 and 4 km (i.e., accumulated data gaps of > 0.25 × 4,000 = 2,000 m), and/or (ii) profiles with > 10 missing data points between the surface and estimated mixing layer height (i.e., accumulated data gaps of > 10 × 20 = 200 m). After data exclusion, 1,897 ozonesondes were available for study: 924 soundings in Beijing and 973 soundings in Hong Kong. Figure 1d shows the monthly distribution of the available ozonesondes.

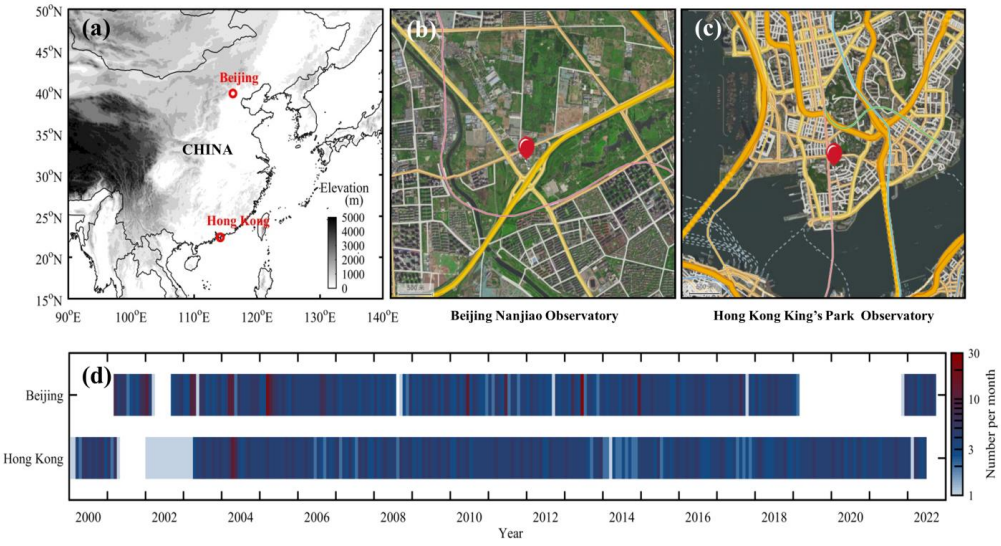

Figure 1. (a) Coordinates and surrounding environments of ozonesonde sites at (b) Beijing Nanjiao Observatory and (c) Hong Kong King's Park Observatory. (d) Monthly distribution of the available ozonesonde observations. Map image is © Amap.

~~**2.2 Space-based ozone precursors**~~

~~Level-3 formaldehyde (CH_2O, an indicator of VOCs) and nitrogen dioxide (NO_2, an indicator of NOx) column products from the Ozone Monitoring Instrument (OMI; https://disc.gsfc.nasa.gov/) were used to characterize O_3 precursor concentrations and diagnose O_3 production sensitivity. OMI is a nadir-looking near-UV/visible CCD spectrometer aboard the Aura satellite of NASA's Earth Observing System (Levelt et al., 2018). It provides global observations from 2004 onwards with a transit time at approximately 13:45 LST. Daily Level-3 products covering the period from 2004 to 2022 were adopted. The spatial resolution of the Level-3 CH_2O products is 0.1° × 0.1°, and that of NO_2 is 0.25° × 0.25°; therefore, a bilinear interpolation method was used to resample OMI products to the~~

~~same resolution (0.25° × 0.25°). We extracted daily data from a 3 × 3 grid region (0.75° × 0.75° centered on the ozonesonde site) and then averaged them to represent O_3 precursor columns for the respective sites.~~

2.~~3~~ 2 Meteorological and a~~A~~tmospheric composition reanalysis

The fifth generation reanalysis (ERA5) data from the European Center for Medium-Range Weather Forecasts (ECMWF) were used to characterize synoptic meteorological conditions. The meteorological variables include geopotential height and horizontal wind vector at 850 hPa, downward ultraviolet radiation at the surface. ERA5 is generated by 4-D variational data assimilation of the ECMWF's Integrated Forecast System and predictions from the CF41R2 model (Hersbach et al., 2020). It has a spatial resolution of 0.25 °× 0.25 °. Besides, ~~the OMI-based column products,~~ pressure-level CH_2O~~,~~ and NO_2 data from the fourth-generation ~~European Center for Medium-Range Weather Forecasts (~~ECMWF~~)~~ Atmospheric Composition Reanalysis (EAC4) were also used to characterize O_3 precursor concentrations and diagnose vertical O_3 production sensitivity. The EAC4 combines model data with global satellite observations into a complete and consistent dataset using a model of the atmosphere based on the laws of physics and chemistry (Inness et al., 2019). It was available at 3-h resolution for a horizontal resolution of 0.75° × 0.75° and a vertical resolution of 7 layers below 700 hPa (1000, 950, 925, 900, 850, 800, and 700 hPa). ~~EAC4 CH_2O and NO_2~~All abovementioned reanalysis data ~~data~~ at 06:00 UTC from 2003 onwards were used to support our interpretation of sonde-based O_3 vertical distribution.

2.~~4~~ 3 Determination of mixing layer top height *h*

Several approaches have been developed to estimate *h* based on the gradient variation of individual atmospheric variables from radiosonde data (Seidel et al., 2010), including temperature (*T*), potential temperature (θ), relative humidity (*RH*), specific humidity (*q*), and atmospheric refractivity (*N*). However, there are substantial differences in the existing methods. Wang and Wang (2014) proposed a three-step method to integrate temperature, humidity, and cloud data to generate a consistent estimate of *h* from radiosonde profiles: Step 1, identify the height (h_0) that best meets the individual criteria for different atmospheric variables; step 2, derive the location of the cloud; and step 3, determine a consistent mixing layer height (h_{con}). We adopted this integral method to determine the mixing layer heights in Beijing and Hong Kong. Five atmospheric variables, namely, *T*, θ, *RH*, *q*, and *N*, were used. Among them, *T* and *RH* were measured by radiosonde, and the other variables were calculated from *T*, *RH,* and atmospheric pressure (Seidel et al., 2010). The upper limit of *h* was set to 4 km.

~~2.5~~2.4 *h*-referenced vertical distribution and classification

Once the mixing layer height *h* was determined, all profiles were expressed in the *z*/*h* vertical coordinate system, where *z* is the actual altitude. In practice, atmospheric variables were interpolated along *z*/*h* values ranging between 0 (the surface) and 2 (2 × *h*) with a vertical resolution of 0.05 (i.e., 41 altitude levels). For instance, if *h* on a specific profile was 1,000 m, the resampled profile extended from 0 to 2000 m with bins of 50 m. Hereafter, this type of vertical profile is denominated as a mixing-layer-height-referenced (i.e., *h*-referenced) profile. In this *z*/*h* vertical coordinate system, mixing-layer O_3 was denominated as MLO_3 and free-tropospheric O_3 was denominated as FTO_3. Based on Student's *t* test, we further classified individual *h*-referenced O_3 profiles into three distinct patterns: MLO_3-dominated (mean MLO_3 significantly higher than mean FTO_3 at a significance level of 0.01); FTO_3-dominated (mean MLO_3 significantly lower than mean FTO_3 at a significance level of 0.01); and uniform distribution (no significant differences between the means of MLO_3 and FTO_3).

2.~~6~~ 5 Diagnosis of ozone production sensitivity

O_3 is photochemically generated when its precursors (e.g., NOx and VOCs) are abundant in the presence of

带格式的：字体：（默认）Times New Roman，五号
带格式的：缩进：首行缩进： 1 字符
带格式的：字体：（默认）Times New Roman，五号
带格式的：字体：（默认）Times New Roman，五号
带格式的：字体：（默认）Times New Roman，五号
带格式的：字体：（默认）Times New Roman，五号
带格式的：字体：（默认）Times New Roman，（中文）宋体，加粗，字体颜色：自定义颜色(RGB(34,34,34))
带格式的：多级符号 + 级别：2 + 编号样式：1，2，3，… + 起始编号：4 + 对齐方式：左侧 + 对齐位置： 0 厘米 + 缩进位置： 0.63 厘米
带格式的：字体：（默认）Times New Roman，加粗

sunlight (Seinfeld and Pandis, 2016). Owing to complex chemical mechanisms and regional differences in emissions and meteorology, the relationship between O_3 and its precursors involves highly non-linear interactions (Jin et al., 2020). Under high VOC and low NOx conditions, O_3 production is not sensitive to VOCs, but is positively correlated to NOx (i.e., a NOx-sensitive regime). Under low VOC and high NOx conditions, O_3 production tends to increase with VOC growth or NOx reduction (i.e., VOC-sensitive regime). In this study, the CH_2O/NO_2 ratio (FNR) was used as the photochemical indicator to diagnose O_3 production sensitivity. An inherent challenge of this diagnosis approach is that FNR thresholds marking the VOC–NOx transition regime are likely distinct from region to region (Jin et al., 2020). For the NCP region (including Beijing), Li et al. (2021) diagnosed the transition regime as occurring when FNR ranges from 1.2 to 2.1; for the PRD region (including Hong Kong), Liao et al. (2021) diagnosed the transition regime as occurring when FNR ranges from 1.0 to 1.5. Ratios below and above these ranges indicate VOC-limited O_3 production and NOx-limited regimes, respectively. These localized FNR thresholds were adopted in this study to diagnose O_3 production sensitivity.

3 Results and discussion

3.1 Lower-tropospheric ozone climatology

Figure 2 shows the traditional lower tropospheric O_3 climatology of Beijing and Hong Kong. Seasonal results are averaged from ozonesonde profiles collected in spring (M–A–M), summer (J–J–A), autumn (S–O–N), and winter (D–J–F). There is a typical summer-high-winter-low seasonality in lower tropospheric O_3 over Beijing, with the highest O_3 concentrations in June. Such seasonality is broadly similar to previous tropospheric O_3 climatology based on lesser O_3 profiles in Beijing (Ding et al., 2008;Zhang et al., 2021). In photochemical active months (May–August), high-concentration O_3 is photochemically produced throughout the lower troposphere, particularly in the mixing layer, causing an isolated O_3-peak area (> 100 ppbv) near the upper mixing layer. In other months, strong urban NO-titration accompanied by weak O_3 production causes a positive vertical gradient of O_3 concentration in the lower troposphere; the average vertical gradient of O_3 reaches a maximum in winter.

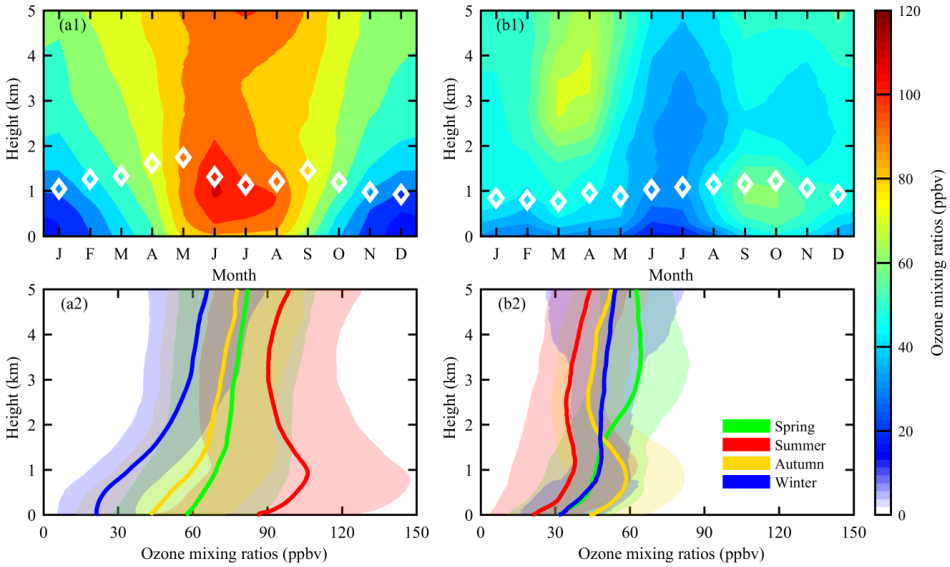

Figure 2. Lower tropospheric ozone vertical distribution over (a) Beijing and (b) Hong Kong. (1) Monthly variation. (2) Seasonal variation. The white diamonds in (1) represent the monthly mean mixing layer height. The

shaded areas in the lower panels denote the standard deviation.

Lower tropospheric O_3 climatology in Hong Kong is remarkably different from that in Beijing. In particular, lower tropospheric O_3 is low in the summertime (< 40 ppbv). Similar O_3 minima have been reported in other subtropical cities in Eastern Asia, such as Hanoi and Naha (Liao et al., 2021;Oltmans et al., 2004;Ogino et al., 2013) and likely reflect the influence of the Asian summer monsoons, which bring maritime air with low O_3 northward from the tropical Pacific to subtropical regions. Although Beijing is also impacted by the Asian summer monsoons, these ocean-sourced air masses become enriched with O_3 precursors while passing over polluted eastern China, leading to an accumulation of O_3 over Beijing. Interestingly, there are two isolated areas of O_3 enhancement over Hong Kong, those in the lower free troposphere (~3.5 km) from March to April and in the upper mixing layer (~0.8 km) in autumn. The former is attributed to long-range transport of wildfire-related O_3 production in the upwind Indochina Peninsula; the latter results from local O_3 production via photochemical reactions under hot and dry weather conditions in autumn (Liao et al., 2021).

3.2 Mixing-layer-height-referenced ozone vertical distribution

We investigated the climatological vertical stratification of O_3 below and above the ML–FT interface (i.e., mixing layer height h) over Beijing and Hong Kong (Fig. 3). This h-referenced O_3 climatology provides an additional dimension (further categorization by mixing layer height) not available in traditional vertical ozone profile climatology. The significant disparity between the h-referenced O_3 climatology (Fig. 3) and traditional O_3 climatology (Fig. 2) illustrates how much information is lost using simple ozonesonde averages. For example, the h-referenced O_3 profiles show a clear inflexion (or discontinuity) at the interface between the ML and FT (z/h=1), which is not apparent in the traditional O_3 climatology. These results reflect the fact that mixing-layer capping inversion acts as an effective although porous geophysical barrier that limits vertical exchange between the ML and FT, leading to distinct O_3 levels on either side.

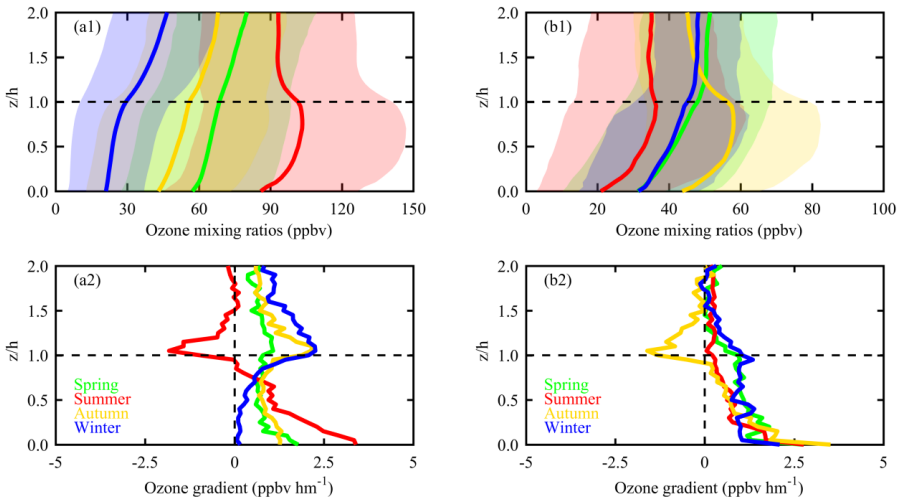

Figure 3. Mixing-layer-height-referenced ozone vertical distribution over (a) Beijing and (b) Hong Kong. (1) Ozone mixing ratio profile. (2) Ozone gradient profile. The shaded areas in the upper panels denote the standard deviation.

In Beijing, seasonal O_3 profiles in autumn, winter, and spring present a low-ML/high-FT vertical distribution

pattern with O_3 mixing ratios that increase with altitude throughout the lower troposphere and variable vertical gradients depending on season and altitude. Generally, the strongest gradients are observed either close to the surface or near the ML–FT interface. Near the surface, they are likely due to strong O_3 titration by NO emitted from urban traffic (Karl et al., 2023). Near the ML–FT interface, they are likely attributable to the barrier effect of mixing-layer capping inversion. The O_3 gradients gradually decrease with altitude above the ML–FT interface; below the interface, they slightly decrease with altitude in spring and autumn but gradually increase with altitude in winter. Winter O_3 gradients are almost zero in the surface layer ($z/h < 0.4$), reflecting strong titration that often causes O_3 to be almost completely depleted in the lower ML. In summer, the averaged O_3 profile exhibits a sickle-shape pattern, with a marked drop in concentrations from the upper ML to the lower FT. Summer O_3 gradients quickly decrease with altitude inside the ML and eventually become negative near the ML–FT interface. The maximum negative gradient (=(-2.2 ppbv hm^{-1}) occurs just above the mixing layer top height. In Hong Kong, the averaged O_3 profiles in winter and spring present low-ML/high-FT vertical distribution, similar to Beijing. However, the autumn averaged O_3 profile shows a sickle-shape pattern, similar to the summer profile in Beijing. In contrast, the summer averaged O_3 profile in Hong Kong displays a transitional feature from spring to autumn, characterized by a weak O_3 peak just below the ML–FT interface. Compared with Beijing, the O_3 gradients in Hong Kong vary across a smaller range; however, they are commonly sharper in the surface layer.

For both Beijing and Hong Kong, the highly variable O_3 gradients in the ML confirm that the well-mixed ML remains a large exception for O_3, even on summer afternoons when vertical turbulent mixing is expected to be strongest. In particular, the increasing O_3 with altitude in the lower ML indicates that strong photochemistry and vertical mixing on summer afternoons is insufficient to quickly compensate for O_3 titration consumption ($NO+O_3 \rightarrow NO_2$) in the surface layer, where NO is largely emitted by urban traffic. A previous study indicated that MLO_3 evolution in urban areas adheres to vertical physiochemical circulation involving multiple reactions in the O_3–NO–NO_2 triad (Tang et al., 2017). NO emissions react with O_3 to generate NO_2 near the ground, which is then transported vertically to the upper ML; O_3 is generated by NO_2 photolysis in the upper ML and is then transported down to the surface layer to compensate for the loss by NO titration. In this process, the titration process is thought to drive the downward flux of O_3 into the urban roughness layer (Karl et al., 2023). Under favorable weather conditions, high-concentration MLO_3 production can greatly modify the vertical profile of O_3 from the more customary low-ML/high-FT vertical distribution to a high-ML/low-FT vertical distribution. This modification is thought to be episodic in low-emission cities (e.g., Frankfurt; (Petetin et al., 2016); in such cities, the vertical structure of averaged O_3 profiles in the photochemical active season (e.g., summer) remains low-ML/high-FT the same throughout the year (Petetin et al., 2018). However, in high-emission megacities (e.g., Beijing and Hong Kong), photochemistry-driven modification can be expected to be common during in the photochemical active season (summer in Beijing and autumn in Hong Kong), eventually causing a seasonal sickle-shape O_3 profile in the lower troposphere. These seasonal differences in lower tropospheric O_3 profiles imply that the aforementioned transport barrier to vertical exchange has different connotations, typically changing from a ML-to-FT detrainment barrier in summer (autumn) to a FT-to-ML entrainment barrier in other seasons in Beijing (Hong Kong).

The vertical autocorrelation of O_3 in the z/h vertical coordinate system was further analyzed to investigate the links between the ML and FT. Based on all individual O_3 profiles, we calculated the correlation coefficients of O_3 between the different pairs of z/h altitude levels. The obtained O_3 vertical autocorrelation matrix is shown in Figure 4. Within both the ML (z/h between 0 and 1) and FT (z/h between 1 and 2), we found strong correlations (usually > 0.90, mean of 0.97 in Beijing; > 0.85, mean of 0.91 in Hong Kong). However, the correlations between the two atmospheric compartments (ML vs. FT) decreased quickly with vertical distance, with means of 0.84 in Beijing and

0.60 in Hong Kong. In general, correlations in Hong Kong were found to be weaker than those in Beijing. This can be explained by two possible reasons. (i) Hong Kong is a coastal city, where clean maritime air and polluted continental air can dominate at different altitudes (e.g., sea-land breeze); therefore, distinct air mass sources can weaken the correlation of O_3 between different altitude levels. (ii) Hong Kong is located in humid zone, where surface sensible heat is relatively weaker than that in semi-humid zones (e.g., Beijing); therefore, weak turbulent convection causes weak mixing of O_3 in the vertical direction (Xu et al., 2021). The iso-correlation contours in both megacities present a "W" shape along the diagonal direction, with the inflexion point at z/h = 1. This is consistent with northern mid-latitude findings in Petetin et al. (2018), indicating that stratification occurs most commonly at the ML–FT interface.

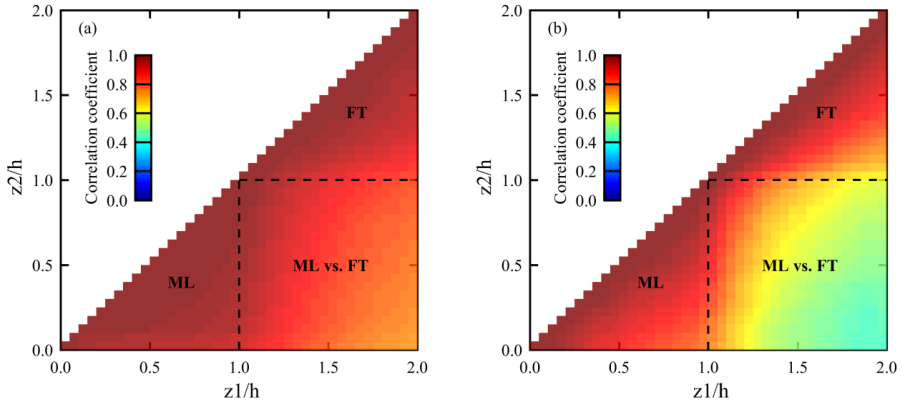

Figure 4. Auto-correlation of ozone mixing ratios between different z/h altitude levels over (a) Beijing and (b) Hong Kong. Dashed lines separate three areas involving correlation within the mixing layer (ML), within the free troposphere (FT), and between the mixing layer and free troposphere (ML vs. FT).

Both surface concentration and vertical distribution of O_3 are highly variable at the synoptic scale and can greatly depart from standard climatology depending on meteorological conditions and the availability of O_3 precursors. Based on Student's *t* test, all individual *h*-referenced O_3 profiles were further classified into three typical patterns to investigate synoptic climatology of lower tropospheric O_3 in Beijing and Hong Kong. The statistical results indicate that the FTO_3-dominated pattern occurs most frequently in both megacities. The respective occurrence frequencies of FTO_3-dominated, uniform, and MLO_3-dominated distributions were 69%, 11%, and 20% in Beijing, and 54%, 21%, and 25% in Hong Kong, respectively. Figure 5 shows the composite of O_3 (gradient) profiles according to the different O_3 profile patterns in Beijing and Hong Kong. In the FTO_3-dominated pattern, averaged FTO_3 concentrations are 61.6 ppbv in Beijing and 44.9 ppbv in Hong Kong, which are 15 and 13 ppbv higher than the averaged MLO_3 concentrations in the respective cities. Such concentration differences between FTO_3 and MLO_3 cause a sharp positive gradient of O_3 near the ML–FT interface (2.3 ppbv hm^{-1} in Beijing and 1.8 ppbv hm^{-1} in Hong Kong). For the MLO_3-dominated pattern, averaged MLO_3 concentrations are 109.8 ppbv in Beijing and 62.2 ppbv in Hong Kong, ~18 ppbv higher than the averaged FTO_3 concentrations in both cities, causing a steep negative gradient of O_3 near the ML–FT interface (−4.3 ppbv hm^{-1} in Beijing and −3.8 ppbv hm^{-1} in Hong Kong). For the uniform distribution, despite no significant difference in the means of MLO_3 and FTO_3, the composited O_3 profile shows an "S" shape pattern with a slightly negative gradient (approximately −1.0 ppbv hm^{-1}) near the ML–FT interface.

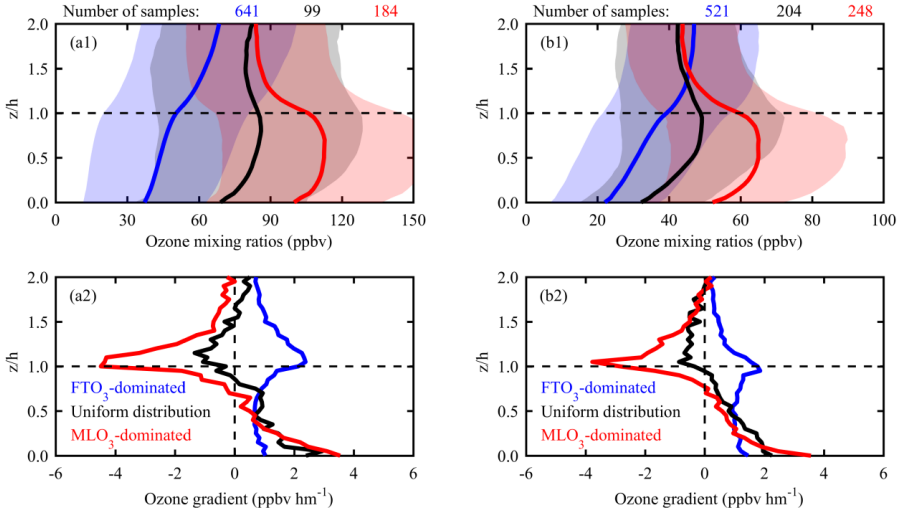

335 Figure 5. Composites of (1) *h*-referenced ozone profiles and (2) *h*-referenced ozone gradient profiles according to different patterns in (a) Beijing and (b) Hong Kong. The shaded areas in the upper panels denote the standard deviation.

Figure 6 shows occurrence frequencies of the three distinct O_3 profile patterns in different seasons and mixing 340 layer height bins. In Beijing, while the FTO_3-dominated pattern prevails in winter (94.2%), autumn (79.1%), and spring (75.3%), the MLO_3-dominated pattern prevails in summer (46.3%). In Hong Kong, the FTO_3-dominated pattern occurs frequently in spring (67.7%), winter (65.8%), and summer (55.8%), and the MLO_3-dominated pattern prevails in autumn (55.1%). Such frequent occurrence of MLO_3-dominated patterns confirms our theory that the MLO_3-dominated pattern is common rather than episodic in the photochemical active season of high- 345 emission Chinese megacities. In contrast, the occurrence dependence of O_3 profile patterns on mixing layer height is not as strong as that on season. The FTO_3-dominated pattern prevails in most *h* bins, particularly in Beijing. Nevertheless, the MLO_3-dominated pattern is still relatively more frequent in the *h* bin between 1.0 and 2.0 km (27.3% in Beijing and 36.7% in Hong Kong) than in lower and higher *h* bins. This is to some degree consistent with the findings of Zhao et al. (2019), who revealed that moderate mixing layer height is usually accompanied by very 350 favorable meteorological (moderate RH and high temperature) and photochemical (NO_x–VOC transition regime) conditions for high-concentration MLO_3 production.

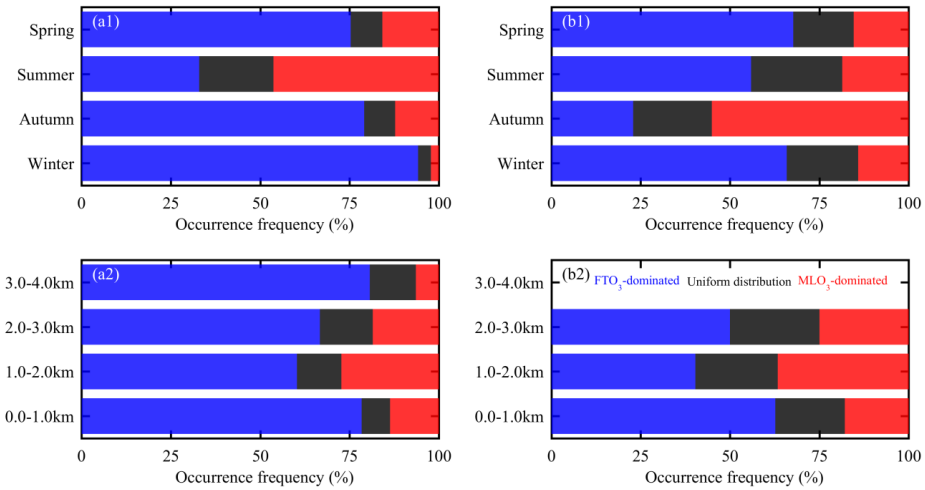

Figure 6. Occurrence frequencies of three *h*-referenced ozone profile patterns according to (1) season and (2) mixing layer height bins in (a) Beijing and (b) Hong Kong (in Hong Kong, no case is found for $h > 3.0$ km).

3.3 Mechanistic understanding of distinct ozone profile patterns in polluted seasons

This section explores the causal mechanisms of distinct O_3 profile patterns in summer of Beijing and autumn of Hong Kong. These two seasons represent the typical ozone-pollution season in individual megacities (Fig. 2). Meanwhile, the days in these two seasons are usually alternately controlled by different O_3 profile pattern, rather than overwhelmingly controlled by single O_3 profile pattern, i.e., FTO_3-dominated pattern (Fig. 6). Therefore, the results focusing on these two seasons will provide a more in-depth understanding of ozone pollution mechanisms through comparison among the different O_3 profile patterns.

Figure 7 shows the composited *h*-referenced O_3 profiles and MLO3 concentrations according to different O_3 profile patterns in summer of Beijing and autumn of Hong Kong. It can be seen that the MLO_3 concentrations present a wide-range variability across the different O_3 profile patterns, while O_3 in the FT part shows a similar concentration, especially in the uppermost part of *h*-referenced lower troposphere, indicating that downward transport of O_3-rich air masses from high altitudes such as stratosphere is not the main factor working to shape the distinct lower-tropospheric O_3 profile patterns. Given the O_3 photochemistry is active in the mixing layer, the wide-range MLO_3 variability indicates that the distinct lower-tropospheric O_3 profile patterns are mainly attributed to varying MLO_3 production, which is modulated by multi-scale meteorology and ozone precursors. In MLO_3-dominated pattern, the medians of MLO_3 concentrations are 117.5 ppbv in Beijing and 61.9 ppbv in Hong Kong, far higher than the corresponding values (66.0 ppbv in Beijing and 33.0 ppbv in Hong Kong) in FTO_3-dominated patterns. This indicates that MLO_3-dominated pattern has a very strong O_3 production through photochemical reaction, whereas FTO_3-dominated pattern corresponds to a weak O_3 production or even a strong O_3 titration ($NO+O_3 \rightarrow NO_2$).

带格式的：字体：非加粗
带格式的：缩进：首行缩进： 1 字符
带格式的：字体：倾斜
带格式的：字体：倾斜
带格式的：字体：非加粗

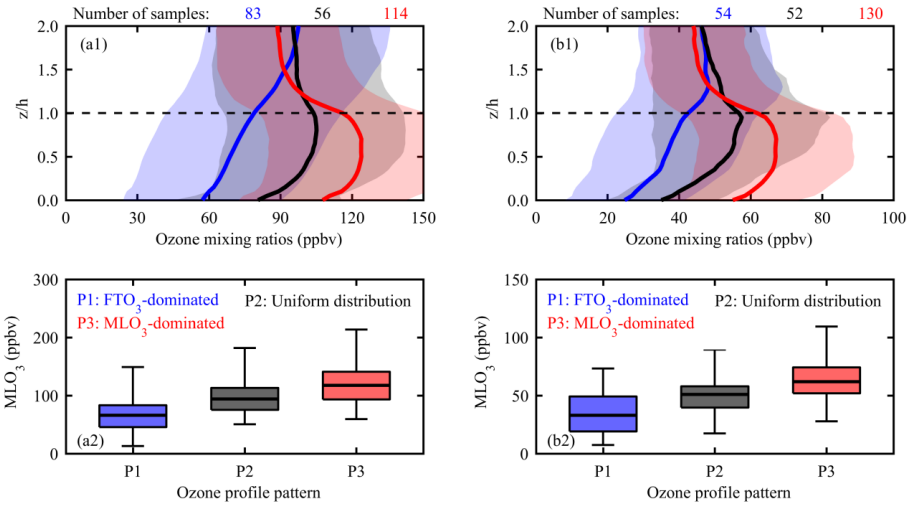

带格式的：字体：（默认）Times New Roman，加粗

Figure 7. (1) Composited *h*-referenced ozone profiles and (2) MLO_3 concentrations according to different ozone profile patterns in (a) summer of Beijing and (b) autumn of Hong Kong. The shaded areas in the upper panels denote the standard deviation. The box-whisker plots in the lower panels denote the MLO_3 concentrations of 2.5, 25, 50, 75, 97.5 percentiles. The digits at the upper of plots denote the sample numbers in each of patterns.

带格式的：字体：非加粗

带格式的：字体：非加粗

3.3.1 Meteorological interpretations

Synoptic meteorological conditions play an important role in controlling lower-tropospheric ozone variability (Kalabokas et al., 2013;Kalabokas et al., 2015;Stauffer et al., 2017). Figure 8 shows the composited large-scale geopotential height and horizontal wind vector at 850 hPa and downward ultraviolet radiation at the surface according to different O_3 profile patterns in summer of Beijing and autumn of Hong Kong.

In summer, ~~the~~ northern China is controlled by continental thermal low-pressure system with prevailing of southerly flows in the North China Plain. The southerly flows are favorable for transporting ozone and its precursors from ~~the~~ central Eastern China to Beijing (Liao et al., 2023), resulting in ozone production and accumulation in the presence of strong ultraviolet radiation. From the FTO_3-dominated to MLO_3-dominated pattern, the low-pressure system is gradually weakened. This change leads to an inhabitation of convective cloud formation, favoring downward ultraviolet radiation. In Fig. 8a, ~~we can see~~there is a slight increase in the downward ultraviolet radiation over northern China from the FTO_3-dominated to MLO_3-dominated pattern, suggesting a tendency toward more favorable photochemical condition. In autumn, ~~the~~ southern China is controlled by weak high-pressure system. From the FTO_3-dominated to MLO_3-dominated pattern, the high-pressure system is gradually strengthened, leading to a significant wind direction change from Pacific-originating easterly flows to continent-originating northeasterly flows over Hong Kong and its surrounding region. The wind direction change causes increasing influence of regional transport of ozone precursors originating from eastern China (Ding et al., 2013). Meanwhile, the strengthened high-pressure system ~~inhibits~~suppresses convective cloud formation, resulting in a significant increase in downward ultraviolet radiation (from 180 kJ m^{-2} to 230 kJ m^{-2}) over Hong Kong and its surrounding region.

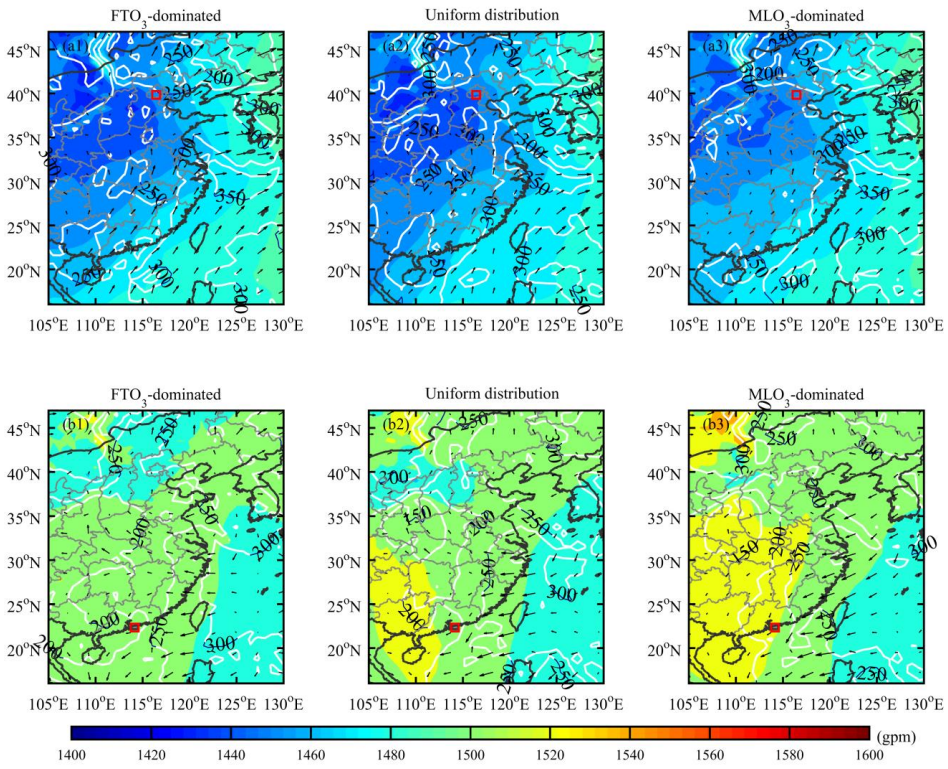

Figure 8. Composited large-scale meteorology, including geopotential height and horizontal wind vector at 850 hPa and downward ultraviolet radiation at the surface (contour, kJ m^{-2}), according to different ozone profile patterns in (a) summer of Beijing and (b) autumn of Hong Kong. The red boxes indicate the locations of Beijing and Hong Kong.

In contrast to large-scale meteorology, local meteorology exerts ~~a~~ more direct influences on local ozone production and accumulation. The *h*-referenced profiles of potential temperature (θ), relative humidity (RH), and wind speed (WS) according to different O_3 profile patterns in summer of Beijing and autumn of Hong Kong are shown in Figure ~~7~~9. Near the surface (z/h < 0.1), potential temperature decreases with altitude in both megacities, indicating a shallow superadiabatic layer due to daytime surface radiation heating. ~~As expected, i~~In other parts of the ML, potential temperature profiles ~~in Beijing~~ are neutral adiabatic (small positive gradient) ~~within the~~due to afternoon convecti~~ve ML~~on (Stull, 1988). However, potential temperature ~~However, the corresponding profiles in Hong Kong are subadiabatic, implying insufficient thermal convection mixing over this coastal city, which may partly explain the lower autocorrelations of O_3 between different altitude levels within the ML in Hong Kong (Fig. 4). I~~in the FT (z/h > 1.0)~~, potential temperature~~ increases with altitude with a ~~relatively~~ larger positive gradient than that in the ML. Particularly, t~~T~~~~As expected, t~~here is a sharp increase in potential temperature at the ML–FT interface where positive vertical gradients reach 1.0 °C hm^{-1} on average. This ~~maximum~~ large gradient is indicative of strong mixing layer capping thermal inversion. However, the maximum gradient values are almost identical among the different O_3 profile patterns, suggesting that capping inversion acts as a transport barrier to suppress O_3 vertical exchange but is not responsible for the different directions of vertical exchange (i.e., FT-to-ML entrainment or ML-to-FT detrainment). Overall~~In fact~~, no significant structural change ~~was~~ is found in the averaged θ profiles

带格式的：字体：（默认）Times New Roman

带格式的：缩进：首行缩进： 0 字符

among the different patterns. Similar to the θ profiles, the RH and WS profiles shared an analogous vertical structure among different O_3 profile patterns in both megacities. In general, RH and WS levels inside the ML were higher and lower, respectively, than the corresponding lower troposphere levels.

Without considering the vertical structure, values of aforementioned meteorological variables usually differ largelyed among the different O_3 profile patterns, suggesting that meteorological conditions are the main regulating factors of lower troposphere O_3 levels. From the the FTO_3-dominated to MLO_3-dominated pattern, there is a significant increase in potential temperature value increases in both megacitiesBeijing. The high temperature of the MLO_3-dominated pattern favors high-concentration ozoneO_3 production in the the MLO_3-dominated pattern. However, there are no significant temperature differences between FTO_3-dominated pattern and MLO_3-dominated pattern in Hong Kong, indicating an insensitivity of Hong Kong's ozone production to air temperature. Turning to relative humidity, it has a significant decrease from the FTO_3-dominated to MLO_3-dominated pattern in both megacities. Given that humid air tends to suppress photochemical reactions (Yu, 2019)(reference), the lower RH in MLO_3-dominated pattern favors ozone photochemical production. In contrast, tThe cross-pattern wind profile value change of RH and WS shows some differences between Beijing and Hong Kong. For example, on MLO_3-dominated days, RH is moderate in Beijing but low in Hong Kong, and when WS is low in Beijing it is moderate in Hong Kong. Nevertheless, RH and WS inside the ML of Hong Kong are always higher than those in the ML of Beijing. While humid air tends to suppress photochemical reactions, windy condition tends to inhibit ozone accumulation. The higher RH and WS conditions may partly explain the lower O_3 levels in Hong Kong. From above analyses a key factor leading to the MLO_3-dominated pattern in both megacities is high temperature. Previous studies have indicated that high temperature not only increases the O_3 production rate (Wang et al., 2022a), but also strengthens the volatilization rate of O_3 precursors, particularly biomass VOC emissions (Duncan et al., 2009). However, there are no significant temperature differences between FTO_3-dominated and MLO_3-dominated pattern in Hong Kong, indicating an insensitivity of Hong Kong's ozone production to air temperature. Turning to relative humidity, it has a significant decrease from FTO_3-dominated pattern to MLO_3-dominated pattern in both megacities. Given that humid air tends to suppress photochemical reactions (Yu, 2019), the lower RH in the MLO_3-dominated pattern favors ozone photochemical production. In contrast to RH, the cross-pattern WS profile change shows some differences between Beijing and Hong Kong. For example, on MLO_3-dominated days, WS is low in Beijing but high in Hong Kong. The high WS conditions indicate that regional transport play an important role in O_3 pollution in Hong Kong. From above analyses a common meteorological factor leading to the MLO_3-dominated pattern in both megacities is low RH.

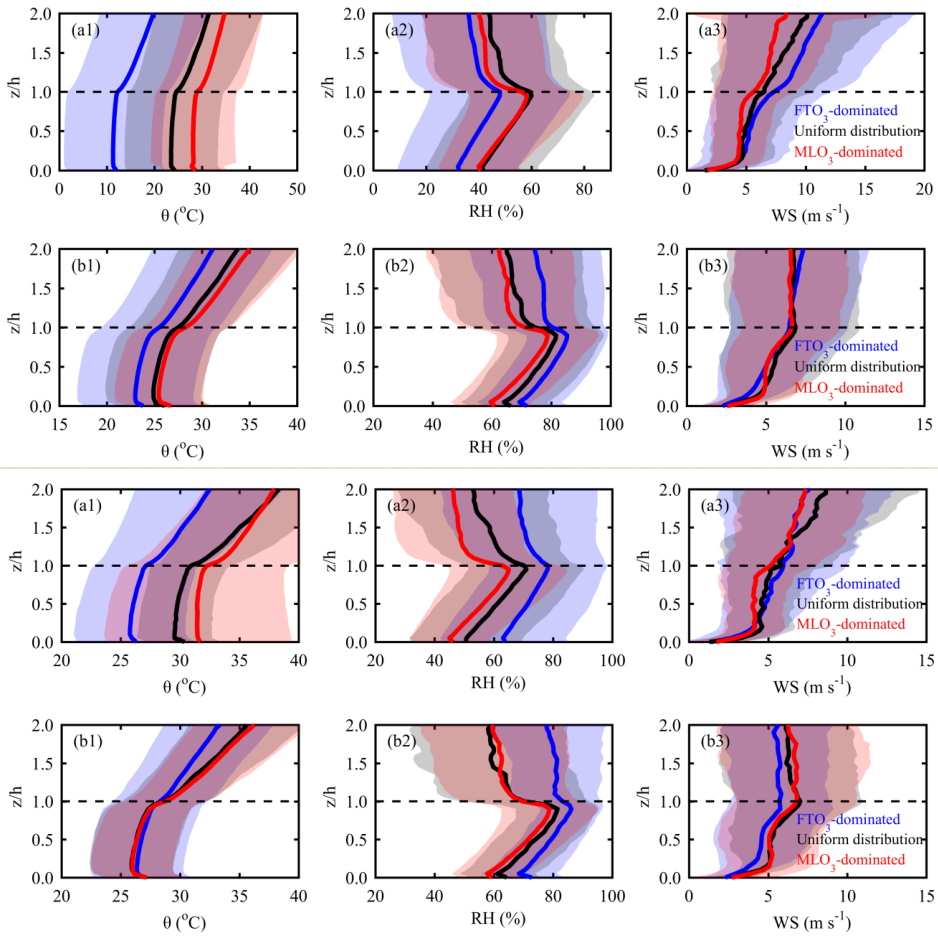

Figure ~~7~~9. Composited *h*-referenced profiles of (1) potential temperature, (2) relative humidity, and (3) wind speed according to different ozone profile patterns in (a) summer of Beijing and (b) autumn of Hong Kong. The shaded areas denote the standard deviation.

3.3.2 Photochemical interpretations

Figure ~~8~~ 10 shows composited ~~column concentrations and~~ vertical distributions of EAC4-based CH_2O and NO_2 concentrations according to the different O_3 profile patterns in summer of Beijing and autumn of Hong Kong. There are significant higher precursor concentrations in Beijing than that in Hong Kong, particularly above the surface layer. This partly explains the higher ozone concentration in Beijing. No matter CH_2O and NO_2, its concentration decreases with altitude in both megacities. By comparison, the vertical gradient of ozone precursors in Hong Kong is significantly larger than that in Beijing. For the different ozone precursors, the vertical gradient of CH_2O is significant smaller than that of NO_2 in the ML part (below 850 hPa). For example, the NO_2 concentration decreases 50-75% (80-85%) from the near surface to 900 hPa in Beijing (Hong Kong), while the corresponding CH_2O concentration just decreases approximately 30% (60%). These vertical characteristics of EAC4-based ozone precursors are consistent with those previous observations (Chi et al., 2018;Lin et al., 2022;Liu et al., 2023).

带格式的：字体：（默认）Times New Roman

带格式的：字体：（默认）Times New Roman

~~. In Beijing, tropospheric CH_2O columns are 7.7 (± 4.3) ×10^{15}, 11.8 (± 6.9) ×10^{15}, and 12.4 (± 5.7) ×10^{15} molec. cm^{-2} in the FTO_3-dominated, uniform distribution, and MLO_3-dominated patterns, respectively; the corresponding values for the tropospheric NO_2 column are 19.2 (± 10.7) ×10^{15}, 14.5 (± 9.8) ×10^{15}, and 13.2 (± 7.7) ×10^{15} molec. cm^{-2}, respectively.~~ From ~~the~~ the FTO_3-dominated ~~pattern~~ to ~~the~~ MLO_3-dominated pattern, CH_2O increases throughout the lower troposphere (up to 700 hPa) in Beijing with a maximum increment in the upper ML (~900 hPa). ~~This~~ The maximum CH_2O increment near the mixing layer top may~~can~~ be explained by ~~high-elevation biogenic VOC emissions in the western mountains (i.e., Taihang Mountains) and~~ northward transport~~vertical mixing~~ of VOC emissions in ~~the southern NCP~~eastern China ~~during the northward transport process~~and high-elevation biogenic VOC emissions in the western mountains (i.e., Taihang Mountains). ~~In contrast~~In contrast to CH_2O, NO_2 ~~mainly~~ decreases in the ~~lower~~ ML part (below 900 hPa), especially in the surface layer (1000 hPa). For example, surface NO_2 concentration is approximately 14 ×10^{-9} kg kg^{-1} in the FTO_3 pattern, but decreases to approximately 9 ×10^{-9} kg kg^{-1} in the MLO_3 pattern. ~~The cross-pattern change of O_3 precursors is likely attributable to significant seasonality of precursor emissions in Beijing and the NCP (e.g., anthropogenic emissions change between heating and non-heating periods and natural emissions change between leafy and leafless periods). As shown in Figure 6, the MLO_3-dominated pattern prevails in the warm season (Spring–Autumn), during which heating-related precursor emissions (mainly NO_x) are negligible but biogenic precursor emissions (mainly VOCs) are considerable (Fig. 7). This explains the elevated CH_2O column and low NO_2 column in the MLO_3-dominated pattern in Beijing.~~

~~In Hong Kong, both CH_2O and NO_2 had lower concentrations than those in Beijing (except for CH_2O in the FTO_3-dominated pattern). This partly explains the lower O_3 levels in Hong Kong.~~ The cross-pattern change of O_3 precursors ~~(regardless of total column or vertical distribution)~~ in Hong Kong nearly follows the same ~~order~~ characteristic as that in Beijing (i.e., increase of CH_2O and decrease of NO_2 from FTO_3-dominated to MLO_3-dominated), but with a significantly smaller change amplitude. This difference is likely attributable to temperature-driven precursor changes. ~~Higher temperatures in the MLO_3-dominated regime trigger the release of VOC emissions, causing higher CH_2O concentrations, and photolysis of NO_2, causing lower NO_2 concentrations.~~In Beijing, the cross-pattern temperature change is very significant. Higher temperatures ~~in the MLO_3-dominated regime~~ in the MLO_3-dominated pattern tends to trigger the release of VOC emissions, causing higher CH_2O concentrations, and to improve the ~~–~~photolysis of NO_2, causing lower NO_2 concentrations. However, the cross-pattern temperature change is insignificant in Hong Kong, leading to small change amplitude of ozone precursors among the different O_3 profile patterns.

~~In Hong Kong, tropospheric CH_2O columns are 8.5 (± 4.8) ×10^{15}, 8.5 (± 3.8) ×10^{15}, and 9.1 (± 4.1) ×10^{15} molec. cm^{-2} in the FTO_3-dominated, uniform distribution, and MLO_3-dominated patterns, respectively. The corresponding values for tropospheric NO_2 columns are 11.8 (± 6.8) ×10^{15}, 11.6 (± 6.8) ×10^{15}, and 11.0 (± 7.6) ×10^{15} molec. cm^{-2}. Evidently, cross-pattern change amplitudes of O_3 precursors in Hong Kong are smaller than those in Beijing. In subtropical Hong Kong and the PRD region, O_3 precursor emissions are not affected by heating-related emission changes from warm to cold season, and are less affected by seasonal biogenic emission changes because of evergreen leaves throughout the year. This weak seasonal dependence of precursor emission leads to small cross-pattern differences in CH_2O and NO_2 in Hong Kong. The slight differences in O_3 precursors among the different O_3 profile patterns in Hong Kong are likely attributable to temperature-driven precursor changes. Higher temperatures in the MLO_3-dominated regime trigger the release of VOC emissions, causing higher CH_2O concentrations, and photolysis of NO_2, causing lower NO_2 concentrations.~~

带格式的：缩进：首行缩进： 0 字符

带格式的：缩进：首行缩进： 0 字符

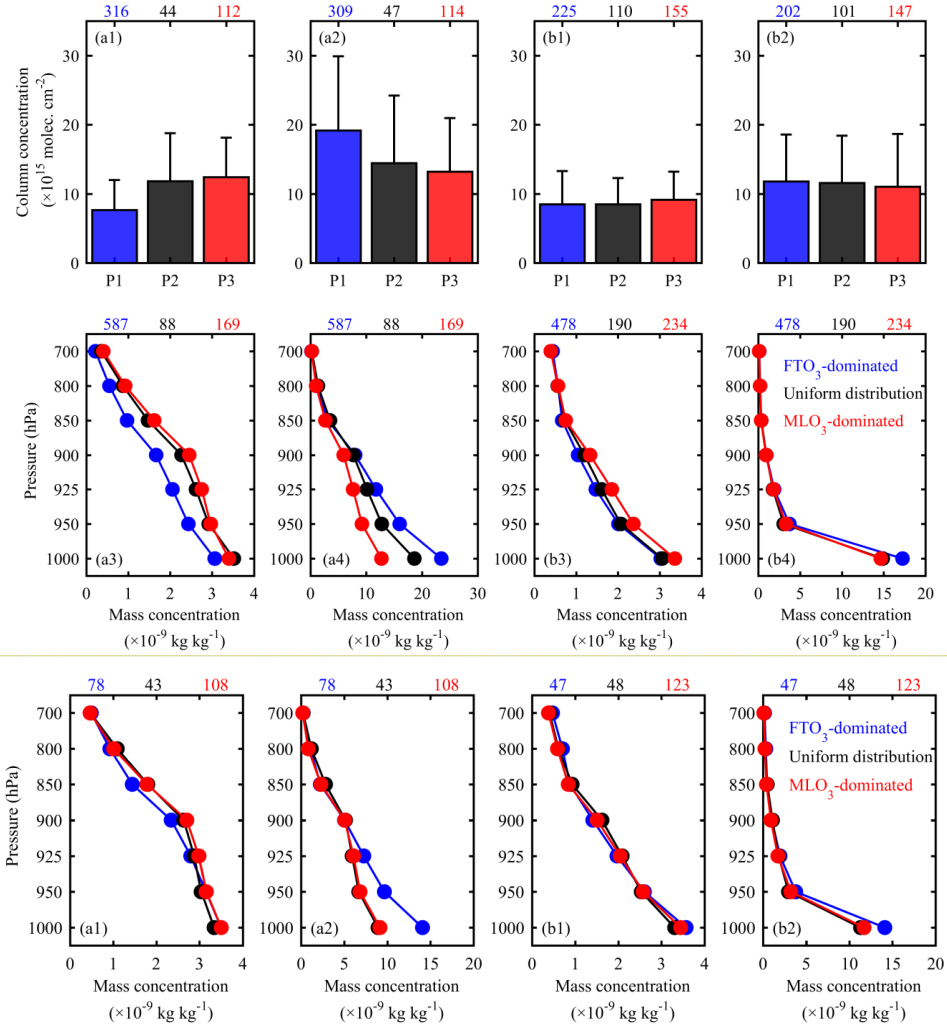

Figure 8110. Composite column concentrations (upper panel) and vertical distributions (lower panel) of ozone precursors (1) CH_2O and (2) NO_2 according to different ozone profile patterns in (a) summer of Beijing and (b) autumn of Hong Kong. The digits at the upper of plots denote the sample numbers in each of patterns. CH_2O (1 and 3); NO_2 (2 and 4). P1: FTO_3-dominated pattern; P2: Uniform distribution pattern; P3: MLO_3-dominated pattern.

Ozone production is nonlinearly dependent on the relative availability of NOx versus VOCs. Owing to the nonlinear relationship between O_3 and its precursors, net production of O_3 is subject to both absolute concentrations of VOC and NOx and their relative ratio, which determines the O_3 production sensitivity. Based on the CH_2O/NO_2 (FNR) photochemical indicator method, we further diagnosed O_3 production sensitivity to examine the potential change in O_3 production chemistryits precursors among different O_3 profile patterns. (

O_3 production chemistry in urban areas is usually VOC limited (Li et al., 2021), and we found that CH_2O concentrations in both Beijing and Hong Kong increased from the FTO_3-dominated to the MLO_3-dominated pattern, suggesting increased potentiality of high-concentration O_3 production. This potentiality can be easily realized on

带格式的: 字体: (默认) Times New Roman

the MLO_3-dominated days owing to the hot-dry weather conditions, providing favorable meteorology for photochemical reactions. That is to say, the MLO_3-dominated pattern in Beijing and Hong Kong is driven by intensive photochemical production of MLO_3 under elevated VOC and high temperature conditions. Since the increment of CH_2O is larger in the upper mixing layer, higher concentration O_3 production can be expected in upper mixing layer, in consistent with the observational result of sickle-shape O_3 profile in the lower troposphere. Conversely, the FTO_3-dominated pattern is likely due to strong titration consumption of MLO_3 under elevated NO_2 and low temperature conditions. Owing to the nonlinear relationship between O_3 and its precursors (i.e., VOC and NOx), net production of O_3 is subject to both absolute concentrations of VOC and NOx and their relative ratio, which determines the O_3 production sensitivity. Based on the FNR photochemical indicator method, we further diagnosed O_3 production sensitivity to examine the potential change in O_3 production chemistry among different O_3 profile patterns.

Figure 9 shows the scatter distribution of OMI-based tropospheric CH_2O and NO_2 columns over Beijing and Hong Kong. In Beijing, most (~90%) points associated with the FTO_3-dominated pattern are located in the VOC-limited regime; these points correspond to high NO_2 concentrations, indicating large O_3 consumption via the titration reaction ($NO+O_3 \rightarrow NO_2$). Strong titration can therefore partly explain the low MLO_3 concentrations in the FTO_3-dominated pattern (another explanation is weak O_3 production due to low temperature). In other patterns, ~27% of days are identified as being in the transition regime, which usually represents optimal VOC-NOx ratios for net production of O_3. High-efficiency O_3 production likely offsets NO titration O_3 consumption, leading to higher MLO_3 concentration compared with that in the FTO_3-dominated pattern. In contrast, in Hong Kong, points that belong to different O_3 profile patterns mix well together, forming similar frequency matrices of O_3 production sensitivity among the different patterns. Compared with the rare occurrence of the NO_x-limited regime in Beijing, the NOx-limited regime is more common in Hong Kong (> 20%), indicating that ozone production chemistry is more sensitive to NO_x in Hong Kong than in Beijing. Since the partly integral concentration of O_3 precursors in the lower layer holds a significantly higher proportion of the total column concentration, the OMI-based analyses are more likely to represent near-surface characteristics of O_3 production sensitivity, particularly in Hong Kong (Fig. 8). Therefore, it is necessary to further explore the vertical characteristics of O_3 production sensitivity.

Figure. 10-11). shows the EAC4-based vertical characteristics of O_3 production sensitivity. In Beijing, the averaged FNR values in the ML (< 850 hPa) differ significantly among the different O_3 profile patterns. However, all are located in the VOC-limited regime. From 850-900 to 700 hPa, the averaged FNR values increase quickly, causing a shift of O_3 production sensitivity from VOC-limited to NOx-limited. Daily statistics indicates that tThere is a significant increase of the transition regime frequency from FTO_3-dominated pattern to MLO_3-dominated pattern, whereas the occurrence of the VOC-limited regime shows an opposite trend. Vertically, the transition regime frequency increases with height in the ML (< 850 hPa), regardless of the O_3 profile pattern. This is broadly similar to the MAX–DOAS-based findings of Chi et al. (2018), who reported that the transition regime accounted for 27.3% at 300 m height, but 50.0% at 1,100 m height over Beijing. In Hong Kong, the averaged FNRFNR values increase more rapidly with height than in Beijing, but show small differences among the different O_3 profile patterns. The shift height of O_3 production sensitivity in Hong Kong (approximately 950 hPa) is lower than that in Beijing. Based on averaged FNR profiles, the shift in Hong Kong occurs in the height range between 950 and 925 hPa. The dDaily occurrence statistics also reveal a higher transition regime frequency in this height range.that bBelow this height, O_3 production chemistry is overwhelmingly controlled by the VOC-limited regime, and above by the NOx-limited regime. Similar results had been reported via MAX–DOAS observations in Guangzhou (a megacity ~110 km northwest of Hong Kong), where O_3 production sensitivity changed with height from VOC-

带格式的：缩进：首行缩进： 0 字符

limited (0.02–0.22 km) to transitional (0.22–0.42 km) to NOx-limited (0.42–2.02 km) (Lin et al., 2022).

Near the surface, O_3 production chemistry is usually VOC-limited in both Beijing and Hong Kong. Controlled by VOC-limited regime, O_3 production increases with increasing VOCs but decreases with NO_x due to titration reaction ($NO + O_3 \rightarrow NO_2$). From the FTO_3-dominated to MLO_3-dominated pattern, NO_2 concentration has a pronounced decrease in both megacities, suggesting a weakening of ozone consumption from NO titration. Meanwhile, CH_2O concentration has a more or less increase, suggesting increased potentiality of high-concentration O_3 production. This potentiality can be easily realized on the MLO_3-dominated days owing to the hot-dry weather conditions, particularly in Beijing. In the upper ML, O_3 production chemistry in Beijing is dominated by VOC-limited and transition regimes. From the FTO_3-dominated to MLO_3-dominated pattern, there is a significant increase in CH_2O concentration in the upper ML of Beijing. Therefore, higher-concentration O_3 production can be expected in upper ML owing to more favorable sensitivity condition, in consistent with the observational result of sickle-shape O_3 profile in the lower troposphere of Beijing. On the contrary, O_3 production chemistry in the upper ML of Hong Kong is dominated by NO_x-limited and transition regimes. From FTO_3-dominated pattern to MLO_3-dominated pattern, there is an insignificant change in NO_2 concentration in the upper ML of Hong Kong. This suggests that the high-concentration MLO_3 in Hong Kong cannot be well explained by local photochemical production. Considering the higher wind speed associated with MLO_3-dominated pattern in Hong Kong (Fig. 9), Regional transport may be an important factor influencing lower-tropospheric ozone distribution over Hong Kong.

~~The above results demonstrate that the ozone precursor level and ozone production sensitivity play an important role in modulating the vertical distribution of O_3 in the lower troposphere. To be specific, the changes of ozone precursor level and ozone production sensitivity determine the final chemical behavior of O_3 (destruction or production) in the mixing layer among the different O_3 profile patterns. In the FTO_3-dominated pattern, the supersaturated NO_x concentrations trigger significant MLO_3 destruction under the overwhelming VOC-limited regime condition, causing a significantly lower O_3 in the mixing layer than that in the free troposphere. Therefore, the mixing layer capping inversion acts as a barrier for FT-to-ML O_3 entrainment in the FTO_3-dmoniated pattern. From the FTO_3-dominated pattern to MLO_3-dominated pattern, the increased CH_2O concentrations push O_3 production sensitivity away from the VOC-limited regime (towards higher NO_x-sensitivity) and favor for ozone photochemically production. The net production of O_3 is expected to be larger in the upper mixing layer, where larger increase of CH_2O occurs. As a result, the MLO_3-dominated pattern is expressed as a sickle-shape O_3 profile (the highest O_3 level in the upper mixing layer), reflecting a ML-to-FT O_3 detrainment barrier effect of mixing layer capping inversion.~~

带格式的： 字体：（中文）宋体，字体颜色：自定义颜色 (RGB(34, 34, 34))

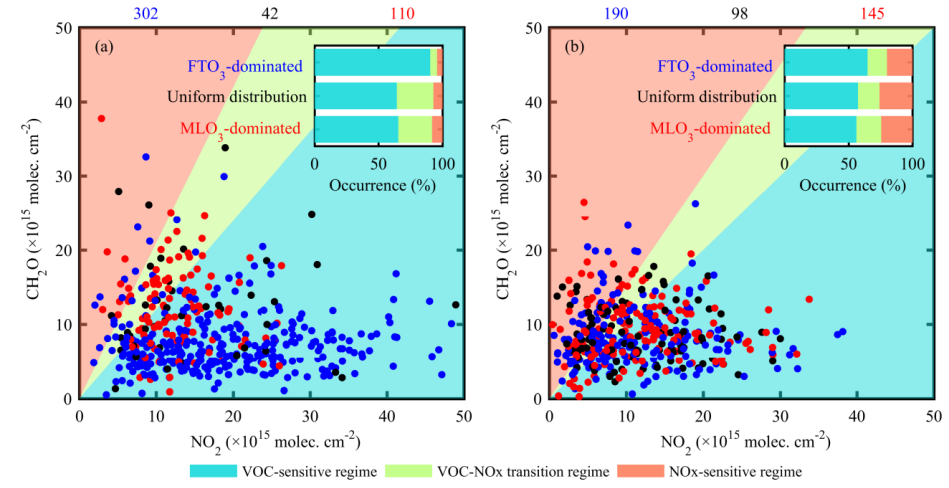

~~Figure 9. Ozone production sensitivity of different ozone profile patterns in (a) Beijing and (b) Hong Kong. Scatter distribution of CH_2O and NO_2 in different ozone production sensitivity regimes (1 and 3); statistical occurrence of daily ozone production sensitivity (2 and 4).~~

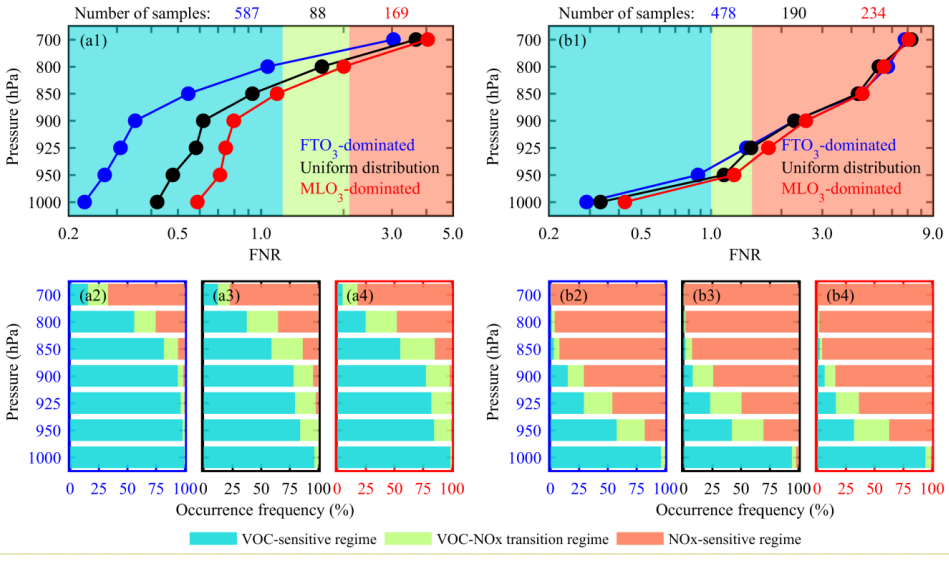

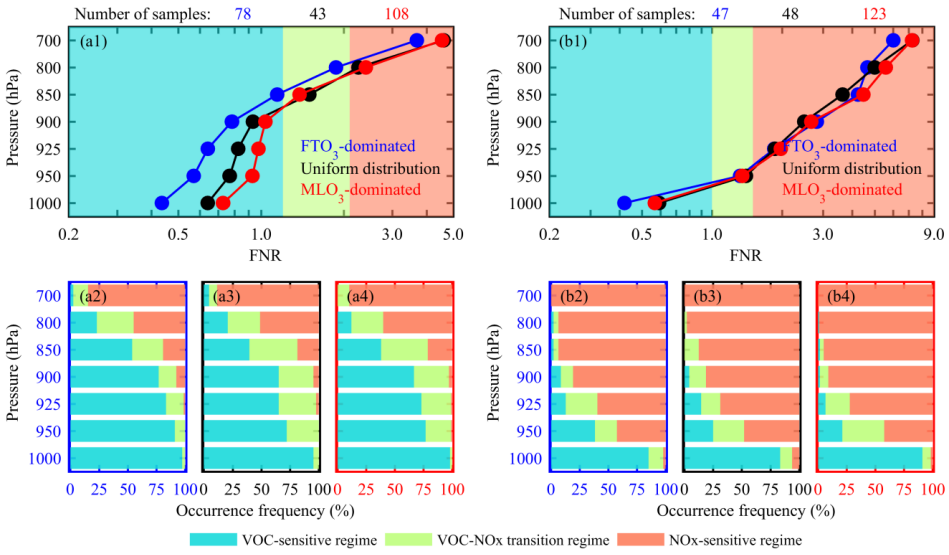

Figure ~~10~~1~~2~~1. Vertical characteristics of ozone production sensitivity according to different ozone profile patterns in (a) summer of Beijing and (b) autumn of Hong Kong. Upper panels (1) denote vertical FNR profiles. Lower panels (2, 3, and 4) denote the occurrence frequency of ozone production sensitivity in FTO_3-dominated, uniform distribution, and MLO_3-dominated patterns. The digits at the upper of plots denote the sample numbers in each of patterns.

4 Summary

We investigate lower tropospheric O_3 distribution over two Chinese megacities (Beijing and Hong Kong) by introducing a novel mixing-layer-height-referenced (*h*-referenced) O_3 climatology, in which lower tropospheric O_3 profiles are scaled according to ~~the~~ mixing layer top height *h*~~s~~. Mixing layer top height was determined by an integral method that integrates temperature, humidity, and cloud profiles. We focused on the lower troposphere (below 2×*h* ~~the mixing layer top height~~), with each profile subdivided in two compartments: the mixing layer and free troposphere (ML and FT). By examining O_3 concentration differences between the ML and FT (i.e., MLO_3 and FTO_3), all individual O_3 profiles were classified into three typical patterns: MLO_3-dominated, FTO_3-dominated, and uniform distribution. ~~Sonde based~~Multi-scale meteorolog~~ical profiles~~y and ~~multi-source~~ O_3 precursors (CH_2O and NO_2) were further analyzed to characterize the main physiochemical processes driving ~~contrasting O_3 budgets among~~ the different O_3 profile patterns in polluted seasons (summer in Beijing and autumn in Hong Kong). Our conclusions are as follows:

带格式的：字体：倾斜

(1) Compared with traditional sea-level-referenced climatology, *h*-referenced O_3 climatology preserves the dependence of O_3 abundance and its variability on mixing layer top height, highlighting an inflexion point (or discontinuity) at the interface between the ML and FT.

(2) ~~Lower tropospheric~~Mixing layer O_3 concentrations show summer-high/winter-low climatology in Beijing, and autumn-high/summer-low climatology in Hong Kong. In the photochemical active season (summer in Beijing and autumn in Hong Kong), seasonal ~~seasonal~~ lower-tropospheric O_3 profiles exhibit a sickle-shape pattern with a marked drop in concentrations from high values in the upper ML to low values in the lower FT. This sickle-shape profile pattern is significantly different from monotone increasing profile patterns

across the rest of the year.

(3) Highly variable O_3 gradients in the lower troposphere, particularly at the surface layer and ML–FT interface, reflect the universality of vertical O_3 stratification structure. O_3 stratification in Hong Kong is stronger than that in Beijing. The stratification in the surface layer is likely due to strong titration chemical processes, and that at the ML–FT interface is attributable to the dynamic transport barrier of mixing layer capping inversion on vertical exchange. The contrasting O_3 gradients at the ML–FT interface indicate different transport barrier effects, which typically shift from a ML-to-FT detrainment barrier in summer (autumn) to a FT-to-ML entrainment barrier in other seasons in Beijing (Hong Kong).

(4) FTO_3-dominated pattern represents the most common O_3 profile patterns in both Beijing and Hong Kong (occurrence frequencies of 69% and 54%, respectively). However, MLO_3-dominated pattern prevails in the photochemical active season, accounting for 46% of summer days in Beijing and 55% of autumn days in Hong Kong, which is more frequent than the previously reported episodic occurrence in northern mid-altitudes, indicating intensive MLO_3 production in high-emission Chinese megacities. In polluted seasons (summer in Beijing and autumn in Hong Kong), the cross-pattern O_3 profiles present a small difference in the FT part but a wide-range variability in the ML part, indicating that MLO_3 production shapes the distinct O_3 profile patterns.

(5) From the FTO_3-dominated to MLO_3-dominated pattern, large-scale meteorology is characterized by increased geopotential height and downward ultraviolet radiation. Locally, t~~T~~here are no vertical structural differences in lower tropospheric meteorological profiles (θ, RH, and WS) among the different O_3 profile patterns. The maximum positive θ gradient at the ML–FT interface demonstrates the common existence of mixing layer capping inversion, which acts as a barrier to vertical exchange. Low humidity represents a common factor associated with MLO_3-dominated pattern in both Beijing and Hong Kong.~~In the FTO_3-dominated pattern, MLO_3 chemistry is dominated by strong titration consumption under low temperature and high NO_2 conditions. Therefore, mixing layer capping inversion acts as a barrier in FT to ML entrainment. In the MLO_3 dominated pattern, MLO3 chemistry is dominated by strong photochemical production under high temperature and high CH_2O conditions. Therefore, mixing layer capping inversion acts as a barrier in ML to FT detrainment.~~

(6) From the FTO_3-dominated to MLO_3-dominated pattern, the O_3 precursor CH_2O (NO_2) substantially increases (decrease) in Beijing, but increases (decreases) slightly in Hong Kong. ~~Over both megacities~~In Beijing, the CH_2O increment is larger in the upper ML, whereas the NO_2 decrement is larger in the lower ML. Such changes in O_3 precursors push O_3 production sensitivity away from the VOC-limited regime (towards higher NO_x sensitivity) and facilitate net production of O_3 via photochemical reactions~~, particularly~~ in the upper ML.

Comparing the above results with previous northern mid-latitude observations (Petetin et al., 2018), lower troposphere O_3 variability over high-emission Chinese megacities is more likely controlled by O_3-related chemical processes, including titration consumption and photochemical production. From our comparison of Beijing and Hong Kong, lower troposphere O_3 variability in China is not only subject to precursor emissions, but also reflects local topographical and meteorological characteristics. Therefore, to achieve comprehensive understanding of lower troposphere O_3 variability in China, more ozonesonde observations over more sites are needed in the future.

Data availability

Ozonesonde data for Beijing are available from the first author upon reasonable request (lzhiheng118@163.com). Ozonesonde data for Hong Kong are available at https://woudc.org/home.php?lang=en.

OMIERA5-based ozone precursormeteorological reanalysis data are available at https://cds.climate.copernicus.eu/https://disc.gsfc.nasa.gov/.

EAC4-based ozone precursor reanalysis data are available at https://ads.atmosphere.copernicus.eu/.

Author contributions

ZL and SF designed the research. ZL organized and wrote the manuscript. MG and JQ edited the manuscript. JS contributed to satellite data analysis and code writing. JZ and YP contributed to ozonesonde observations in Beijing. All authors contributed to the revision of the manuscript.

Competing interests

The contact author has declared that none of the authors has any competing interests.

Disclaimer

Publisher's note: Copernicus Publications remains neutral with regard to jurisdictional claims in published maps and institutional affiliations.

Financial support

This work is supported by the major project of Basic and Applied Basic Research project of Guangdong Province (grant no. 2020B0301030004), the Key-Area Research and Development Program of Guangdong Province (grant no. 2020B1111360003), the National Natural Science Foundation of China (grant no. 42293321 and 41975181).

References

Benish, S. E., He, H., Ren, X. R., Roberts, S. J., Salawitch, R. J., Li, Z. Q., Wang, F., Wang, Y. Y., Zhang, F., Shao, M., Lu, S. H., and Dickerson, R. R.: Measurement report: Aircraft observations of ozone, nitrogen oxides, and volatile organic compounds over Hebei Province, China, Atmos Chem Phys, 20, 14523-14545, 10.5194/acp-20-14523-2020, 2020.

Berkes, F., Hoor, P., Bozem, H., Kunkel, D., Sprenger, M., and Henne, S.: Airborne observation of mixing across the entrainment zone during PARADE 2011, Atmos. Chem. Phys., 16, 6011-6025, 10.5194/acp-16-6011-2016, 2016.

Chen, Z., Xie, Y., Liu, J., Shen, L., Cheng, X., Han, H., Yang, M., Shen, Y., Zhao, T., and Hu, J.: Distinct seasonality in vertical variations of tropospheric ozone over coastal regions of southern China, Sci Total Environ, 874, 162423, https://doi.org/10.1016/j.scitotenv.2023.162423, 2023.

Chi, X. Y., Liu, C., Xie, Z. Q., Fan, G. Q., Wang, Y., He, P. Z., Fan, S. D., Hong, Q. Q., Wang, Z., Yu, X. W., Yue, F. E., Duan, J. B., Zhang, P. F., and Liu, J. G.: Observations of ozone vertical profiles and corresponding precursors in the low troposphere in Beijing, China, Atmos Res, 213, 224-235, 10.1016/j.atmosres.2018.06.012, 2018.

Diab, R. D., Thompson, A. M., Mari, K., Ramsay, L., and Coetzee, G. J. R.: Tropospheric ozone climatology over Irene, South Africa, from 1990 to 1994 and 1998 to 2002, J Geophys Res-Atmos, 109, Artn D20301 10.1029/2004jd004793, 2004.

Ding, A. J., Wang, T., Thouret, V., Cammas, J. P., and Nedelec, P.: Tropospheric ozone climatology over Beijing: analysis of aircraft data from the MOZAIC program, Atmos Chem Phys, 8, 1-13, Doi 10.5194/Acp-8-1-2008, 2008.

Ding, A. J., Wang, T., and Fu, C. B.: Transport characteristics and origins of carbon monoxide and ozone in Hong Kong, South China, J Geophys Res-Atmos, 118, 9475-9488, 10.1002/jgrd.50714, 2013.

Donnell, E. A., Fish, D. J., Dicks, E. M., and Thorpe, A. J.: Mechanisms for pollutant transport between the boundary layer and the free troposphere, Journal of Geophysical Research: Atmospheres, 106, 7847-7856, https://doi.org/10.1029/2000JD900730, 2001.

Duncan, B. N., Yoshida, Y., Damon, M. R., Douglass, A. R., and Witte, J. C.: Temperature dependence of factors controlling

isoprene emissions, Geophysical Research Letters, 36, https://doi.org/10.1029/2008GL037090, 2009.

Fleming, Z. L., Doherty, R. M., von Schneidemesser, E., Malley, C. S., Cooper, O. R., Pinto, J. P., Colette, A., Xu, X. B., Simpson, D., Schultz, M. G., Lefohn, A. S., Hamad, S., Moolla, R., Solberg, S., and Feng, Z. Z.: Tropospheric Ozone Assessment Report: Present-day ozone distribution and trends relevant to human health, Elementa-Sci Anthrop, 6, Artn 12
10.1525/Elementa.273, 2018.

Han, S., Yao, Q., Tie, X., Zhang, Y., Zhang, M., Li, P., and Cai, Z.: Analysis of surface and vertical measurements of O3 and its chemical production in the NCP region, China, Atmos Environ, 241, 117759, https://doi.org/10.1016/j.atmosenv.2020.117759, 2020.

He, G. W., Deng, T., Wu, D., Wu, C., Huang, X. F., Li, Z. N., Yin, C. Q., Zou, Y., Song, L., Ouyang, S. S., Tao, L. P., and Zhang, X.: Characteristics of boundary layer ozone and its effect on surface ozone concentration in Shenzhen, China: A case study, Sci Total Environ, 791, ARTN 148044
10.1016/j.scitotenv.2021.148044, 2021.

Hersbach, H., Bell, B., Berrisford, P., Hirahara, S., Horanyi, A., Munoz-Sabater, J., Nicolas, J., Peubey, C., Radu, R., Schepers, D., Simmons, A., Soci, C., Abdalla, S., Abellan, X., Balsamo, G., Bechtold, P., Biavati, G., Bidlot, J., Bonavita, M., De Chiara, G., Dahlgren, P., Dee, D., Diamantakis, M., Dragani, R., Flemming, J., Forbes, R., Fuentes, M., Geer, A., Haimberger, L., Healy, S., Hogan, R. J., Holm, E., Janiskova, M., Keeley, S., Laloyaux, P., Lopez, P., Lupu, C., Radnoti, G., de Rosnay, P., Rozum, I., Vamborg, F., Villaume, S., and Thepaut, J. N.: The ERA5 global reanalysis, Q J Roy Meteor Soc, 146, 1999-2049, 10.1002/qj.3803, 2020.

Inness, A., Ades, M., Agustí-Panareda, A., Barré, J., Benedictow, A., Blechschmidt, A. M., Dominguez, J. J., Engelen, R., Eskes, H., Flemming, J., Huijnen, V., Jones, L., Kipling, Z., Massart, S., Parrington, M., Peuch, V. H., Razinger, M., Remy, S., Schulz, M., and Suttie, M.: The CAMS reanalysis of atmospheric composition, Atmos. Chem. Phys., 19, 3515-3556, 10.5194/acp-19-3515-2019, 2019.

Jaffe, D.: Relationship between Surface and Free Tropospheric Ozone in the Western U.S., Environ Sci Technol, 45, 432-438, 10.1021/es1028102, 2011.

Jin, X. M., Fiore, A., Boersma, K. F., De Smedt, I., and Valin, L.: Inferring Changes in Summertime Surface Ozone-NOx-VOC Chemistry over US Urban Areas from Two Decades of Satellite and Ground-Based Observations, Environ Sci Technol, 54, 6518-6529, 10.1021/acs.est.9b07785, 2020.

Kalabokas, P. D., Cammas, J. P., Thouret, V., Volz-Thomas, A., Boulanger, D., and Repapis, C. C.: Examination of the atmospheric conditions associated with high and low summer ozone levels in the lower troposphere over the eastern Mediterranean, Atmos Chem Phys, 13, 10339-10352, 10.5194/acp-13-10339-2013, 2013.

Kalabokas, P. D., Thouret, V., Cammas, J. P., Volz-Thomas, A., Boulanger, D., and Repapis, C. C.: The geographical distribution of meteorological parameters associated with high and low summer ozone levels in the lower troposphere and the boundary layer over the eastern Mediterranean (Cairo case), Tellus B, 67, Artn 27853
10.3402/Tellusb.V67.27853, 2015.

Karl, T., Lamprecht, C., Graus, M., Cede, A., Tiefengraber, M., Vila-Guerau de Arellano, J., Gurarie, D., and Lenschow, D.: High urban NOx triggers a substantial chemical downward flux of ozone, Science Advances, 9, eadd2365, 10.1126/sciadv.add2365, 2023.

Kaser, L., Patton, E. G., Pfister, G. G., Weinheimer, A. J., Montzka, D. D., Flocke, F., Thompson, A. M., Stauffer, R. M., and Halliday, H. S.: The effect of entrainment through atmospheric boundary layer growth on observed and modeled surface ozone in the Colorado Front Range, J Geophys Res-Atmos, 122, 6075-6093, 10.1002/2016JD026245, 2017.

Li, R. Y., Xu, M. Q., Li, M. C., Chen, Z. Y., Zhao, N., Gao, B. B., and Yao, Q.: Identifying the spatiotemporal variations in ozone formation regimes across China from 2005 to 2019 based on polynomial simulation and causality analysis, Atmos Chem Phys, 21, 15631-15646, 10.5194/acp-21-15631-2021, 2021.

Liao, Z., Ling, Z., Gao, M., Sun, J., Zhao, W., Ma, P., Quan, J., and Fan, S.: Tropospheric Ozone Variability Over Hong Kong Based on Recent 20 years (2000–2019) Ozonesonde Observation, Journal of Geophysical Research: Atmospheres, 126, e2020JD033054, https://doi.org/10.1029/2020JD033054, 2021.

Liao, Z. H., Pan, Y. B., Ma, P. K., Jia, X. C., Cheng, Z. G., Wang, Q. Q., Dou, Y. J., Zhao, X. J., Zhang, J. Q., and Quan, J. N.: Meteorological and chemical controls on surface ozone diurnal variability in Beijing: A clustering-based perspective, Atmos Environ, 295, ARTN 119566
10.1016/j.atmosenv.2022.119566, 2023.

Lin, C. H., Wu, Y. L., and Lai, C. H.: Ozone reservoir layers in a coastal environment - a case study in southern Taiwan, Atmos. Chem. Phys., 10, 4439-4452, 10.5194/acp-10-4439-2010, 2010.

Lin, H., Xing, C., Hong, Q., Liu, C., Ji, X., Liu, T., Lin, J., Lu, C., Tan, W., Li, Q., and Liu, H.: Diagnosis of Ozone Formation Sensitivities in Different Height Layers via MAX‐DOAS Observations in Guangzhou, Journal of Geophysical Research: Atmospheres, 127, 10.1029/2022jd036803, 2022.

Liu, Z., Zha, F., Wang, Y., Yuan, B., Liu, B., and Tang, G.: Vertical evolution of the concentrations and sources of volatile organic compounds in the lower boundary layer in urban Beijing in summer, Chemosphere, 332, 138767, https://doi.org/10.1016/j.chemosphere.2023.138767, 2023.

Lu, X., Hong, J. Y., Zhang, L., Cooper, O. R., Schultz, M. G., Xu, X. B., Wang, T., Gao, M., Zhao, Y. H., and Zhang, Y. H.: Severe Surface Ozone Pollution in China: A Global Perspective, Environ Sci Tech Let, 5, 487-494, 10.1021/acs.estlett.8b00366, 2018.

Mills, G., Pleijel, H., Malley, C. S., Sinha, B., Cooper, O. R., Schultz, M. G., Neufeld, H. S., Simpson, D., Sharps, K., Feng, Z. Z., Gerosa, G., Harmens, H., Kobayashi, K., Saxena, P., Paoletti, E., Sinha, V., and Xu, X. B.: Tropospheric Ozone Assessment Report: Present-day tropospheric ozone distribution and trends relevant to vegetation, Elementa-Sci Anthrop, 6, Artn 47
10.1525/Elementa.302, 2018.

Monks, P. S., Archibald, A. T., Colette, A., Cooper, O., Coyle, M., Derwent, R., Fowler, D., Granier, C., Law, K. S., Mills, G. E., Stevenson, D. S., Tarasova, O., Thouret, V., von Schneidemesser, E., Sommariva, R., Wild, O., and Williams, M. L.: Tropospheric ozone and its precursors from the urban to the global scale from air quality to short-lived climate forcer, Atmos Chem Phys, 15, 8889-8973, 10.5194/acp-15-8889-2015, 2015.

Neuman, J. A., Trainer, M., Aikin, K. C., Angevine, W. M., Brioude, J., Brown, S. S., de Gouw, J. A., Dube, W. P., Flynn, J. H., Graus, M., Holloway, J. S., Lefer, B. L., Nedelec, P., Nowak, J. B., Parrish, D. D., Pollack, I. B., Roberts, J. M., Ryerson, T. B., Smit, H., Thouret, V., and Wagner, N. L.: Observations of ozone transport from the free troposphere to the Los Angeles basin, Journal of Geophysical Research: Atmospheres, 117, https://doi.org/10.1029/2011JD016919, 2012.

Ogino, S. Y., Fujiwara, M., Shiotani, M., Hasebe, F., Matsumoto, J., Hoang, T. H. T., and Nguyen, T. T. T.: Ozone variations over the northern subtropical region revealed by ozonesonde observations in Hanoi, J Geophys Res-Atmos, 118, 3245-3257, 10.1002/jgrd.50348, 2013.

Oltmans, S. J., Johnson, B. J., Harris, J. M., Thompson, A. M., Liu, H. Y., Chan, C. Y., Vomel, H., Fujimoto, T., Brackett, V. G., Chang, W. L., Chen, J. P., Kim, J. H., Chan, L. Y., and Chang, H. W.: Tropospheric ozone over the North Pacific from ozonesonde observations, J Geophys Res-Atmos, 109, Artn D15s01
10.1029/2003jd003466, 2004.

Petetin, H., Thouret, V., Fontaine, A., Sauvage, B., Athier, G., Blot, R., Boulanger, D., Cousin, J. M., and Nédélec, P.: Characterising tropospheric O3 and CO around Frankfurt over the period 1994–2012 based on MOZAIC–IAGOS aircraft measurements, Atmos. Chem. Phys., 16, 15147-15163, 10.5194/acp-16-15147-2016, 2016.

Petetin, H., Sauvage, B., Smit, H. G. J., Gheusi, F., Lohou, F., Blot, R., Clark, H., Athier, G., Boulanger, D., Cousin, J. M., Nedelec, P., Neis, P., Rohs, S., and Thouret, V.: A climatological view of the vertical stratification of RH, O3 and CO within the PBL and at the interface with free troposphere as seen by IAGOS aircraft and ozonesondes at northern mid-latitudes

over 1994–2016, Atmos. Chem. Phys., 18, 9561-9581, 10.5194/acp-18-9561-2018, 2018.

Seidel, D. J., Ao, C. O., and Li, K.: Estimating climatological planetary boundary layer heights from radiosonde observations: Comparison of methods and uncertainty analysis, Journal of Geophysical Research: Atmospheres, 115, https://doi.org/10.1029/2009JD013680, 2010.

Seinfeld, J. H., and Pandis, S. N.: Atmospheric Chemistry and Physics from Air Pollution to Climate Change, third ed. John, W., Sons, Inc., 2016.

Stauffer, R. M., Thompson, A. M., and Young, G. S.: Tropospheric ozonesonde profiles at long-term US monitoring sites: 1. A climatology based on self-organizing maps, J Geophys Res-Atmos, 121, 1320-1339, 10.1002/2015JD023641, 2016.

Stauffer, R. M., Thompson, A. M., Oltmans, S. J., and Johnson, B. J.: Tropospheric ozonesonde profiles at long-term US monitoring sites: 2. Links between Trinidad Head, CA, profile clusters and inland surface ozone measurements, J Geophys Res-Atmos, 122, 1261-1280, 10.1002/2016JD025254, 2017.

Stull, R. B.: An Introduction to Boundary Layer Meteorology; Kluwer Academic Publishers, Dordrecht, The Netherlands., 1988.

Tang, G. Q., Zhu, X. W., Xin, J. Y., Hu, B., Song, T., Sun, Y., Zhang, J. Q., Wang, L. L., Cheng, M. T., Chao, N., Kong, L. B., Li, X., and Wang, Y. S.: Modelling study of boundary-layer ozone over northern China - Part I: Ozone budget in summer, Atmos Res, 187, 128-137, 10.1016/j.atmosres.2016.10.017, 2017.

Trousdell, J. F., Conley, S. A., Post, A., and Faloona, I. C.: Observing entrainment mixing, photochemical ozone production, and regional methane emissions by aircraft using a simple mixed-layer framework, Atmos. Chem. Phys., 16, 15433-15450, 10.5194/acp-16-15433-2016, 2016.

Wang, P., Yang, Y., Li, H., Chen, L., Dang, R., Xue, D., Li, B., Tang, J., Leung, L. R., and Liao, H.: North China Plain as a hot spot of ozone pollution exacerbated by extreme high temperatures, Atmos. Chem. Phys., 22, 4705-4719, 10.5194/acp-22-4705-2022, 2022a.

Wang, T., Xue, L., Brimblecombe, P., Lam, Y. F., Li, L., and Zhang, L.: Ozone pollution in China: A review of concentrations, meteorological influences, chemical precursors, and effects, Sci Total Environ, 575, 1582-1596, https://doi.org/10.1016/j.scitotenv.2016.10.081, 2017.

Wang, T., Xue, L., Feng, Z., Dai, J., Zhang, Y., and Tan, Y.: Ground-level ozone pollution in China: a synthesis of recent findings on influencing factors and impacts, Environmental Research Letters, 17, 063003, 10.1088/1748-9326/ac69fe, 2022b.

Wang, X. Y., and Wang, K. C.: Estimation of atmospheric mixing layer height from radiosonde data, Atmos. Meas. Tech., 7, 1701-1709, 10.5194/amt-7-1701-2014, 2014.

Williams, A. G., Zahorowski, W., Chambers, S., Griffiths, A., Hacker, J. M., Element, A., and Werczynski, S.: The Vertical Distribution of Radon in Clear and Cloudy Daytime Terrestrial Boundary Layers, Journal of the Atmospheric Sciences, 68, 155-174, https://doi.org/10.1175/2010JAS3576.1, 2011.

Wyngaard, J. C., and Brost, R. A.: Top-Down and Bottom-Up Diffusion of a Scalar in the Convective Boundary Layer, Journal of Atmospheric Sciences, 41, 102-112, https://doi.org/10.1175/1520-0469(1984)041<0102:TDABUD>2.0.CO;2, 1984.

Xu, Z., Chen, H., Guo, J., and Zhang, W.: Contrasting Effect of Soil Moisture on the Daytime Boundary Layer Under Different Thermodynamic Conditions in Summer Over China, Geophysical Research Letters, 48, e2020GL090989, https://doi.org/10.1029/2020GL090989, 2021.

Yates, E. L., Johnson, M. S., Iraci, L. T., Ryoo, J. M., Pierce, R. B., Cullis, P. D., Gore, W., Ives, M. A., Johnson, B. J., Leblanc, T., Marrero, J. E., Sterling, C. W., and Tanaka, T.: An Assessment of Ground Level and Free Tropospheric Ozone Over California and Nevada, Journal of Geophysical Research: Atmospheres, 122, 10,089-010,102, https://doi.org/10.1002/2016JD026266, 2017.

Yonemura, S., Tsuruta, H., Kawashima, S., Sudo, S., Peng, L. C., Fook, L. S., Johar, Z., and Hayashi, M.: Tropospheric ozone

climatology over Peninsular Malaysia from 1992 to 1999, Journal of Geophysical Research: Atmospheres, 107, ACH 1-1-ACH 1-12, https://doi.org/10.1029/2001JD000993, 2002.

Yu, S. C.: Fog geoengineering to abate local ozone pollution at ground level by enhancing air moisture, Environ Chem Lett, 17, 565-580, 10.1007/s10311-018-0809-5, 2019.

Zhang, J., Li, D., Bian, J., Xuan, Y., Chen, H., Bai, Z., Wan, X., Zheng, X., Xia, X., and Lü, D.: Long-term ozone variability in the vertical structure and integrated column over the North China Plain: results based on ozonesonde and Dobson measurements during 2001–2019, Environmental Research Letters, 16, 074053, 10.1088/1748-9326/ac109f, 2021.

Zhao, W., Tang, G. Q., Yu, H., Yang, Y., Wang, Y. H., Wang, L. L., An, J. L., Gao, W. K., Hu, B., Cheng, M. T., An, X. Q., Li, X., and Wang, Y. S.: Evolution of boundary layer ozone in Shijiazhuang, a suburban site on the North China Plain, J Environ Sci, 83, 152-160, 10.1016/j.jes.2019.02.016, 2019.

Zhu, X. W., Ma, Z. Q., Qiu, Y. L., Liu, H., Liu, Q., and Yin, X. M.: An evaluation of the interaction of morning residual layer ozone and mixing layer ozone in rural areas of the North China Plain, Atmos Res, 236, ARTN 104788 10.1016/j.atmosres.2019.104788, 2020.